1	A positive allosteric modulator of the $\beta_1AR$ with antagonist activity for catecholaminergic
2	polymorphic ventricular tachycardia
3	
4	Alyssa Grogan <sup>1</sup> , Robin M. Perelli* <sup>2,3</sup> , Seungkirl Ahn* <sup>1</sup> , Haoran Jiang <sup>1</sup> , Arun Jyothidasan <sup>1</sup> ,
5	Damini Sood <sup>1</sup> , Chongzhao You <sup>1</sup> , David I. Israel <sup>4</sup> , Alex Shaginian <sup>4</sup> , Qiuxia Chen <sup>4</sup> , Jian Liu <sup>4</sup> , Jialu
6	Wang <sup>1</sup> , Jan Steyaert <sup>5,6</sup> , Alem W. Kahsai <sup>1</sup> , Andrew P. Landstrom <sup>2,3</sup> , Robert J. Lefkowitz <sup>1,7,8</sup> , and
7	Howard A. Rockman <sup>1,2,#</sup>
8	
9	<sup>1</sup> Department of Medicine, Duke University Medical Center
10	<sup>2</sup> Department of Cell Biology, Duke University Medical Center
11	<sup>3</sup> Division of Cardiology, Department of Pediatrics, Duke University School of Medicine
12	<sup>4</sup> HitGen Inc, Chengdu, China
13	<sup>5</sup> VIB-VUB Center for Structural Biology, VIB, pleinlaan 2, 1050 Brussels, Belgium
14	<sup>6</sup> Structural Biology Brussels, Vrije Universiteit Brussel, Pleinlaan 2, 1050 Brussels, Beglium
15	<sup>7</sup> Department of Biochemistry, Duke University Medical Center
16	<sup>8</sup> Howard Hughes Medical Institute, Duke University Medical Center
17	* Authors contributed equally
18	# Correspondence to: Howard A. Rockman, MD.,
19	Department of Medicine, Duke University Medical Center,
20	DUMC 3104, 226 CARL Building,
21	Durham, NC 27710,
22	Email: h.rockman@duke.edu
23	

#### Abstract:

24

25

26

27

28

29

30

31

32

33

34

35

36

37

38

39

40

41

42

Orthosteric β-blockers represent the leading pharmacological intervention for managing heart diseases owing to their ability to competitively antagonize β-adrenergic receptors (βARs). However, their use is often limited by the development of adverse effects such as fatigue, hypotension, and reduced exercise capacity, due in part to the nonselective inhibition of multiple βAR subtypes. These challenges are particularly problematic in treating catecholaminergic polymorphic ventricular tachycardia (CPVT), a disease characterized by lethal tachyarrhythmias directly triggered by cardiac β<sub>1</sub>AR activation. To identify small molecule allosteric modulators of the  $\beta_1AR$  that could offer enhanced subtype specificity and robust functional antagonism of  $\beta_1AR$ mediated signaling, we conducted a DNA-encoded small molecule library screen and discovered Compound 11 (C11). C11 selectively potentiates the binding affinity of orthosteric agonists to the β<sub>1</sub>AR while potently *inhibiting* downstream signaling following β<sub>1</sub>AR activation. Moreover, C11 prevents agonist-induced spontaneous contractile activity, Ca<sup>2+</sup> release events, and exerciseinduced ventricular tachycardia in the CSQ2<sup>-/-</sup> murine model of CPVT. Collectively, our studies demonstrate that C11 belongs to an emerging class of allosteric modulators termed PAMantagonists that positively modulate agonist binding but block downstream function. With unique pharmacological properties and selective functional antagonism of  $\beta_1$ AR-mediated signaling, C11 represents a promising therapeutic candidate for the treatment of CPVT and other forms of cardiac disease associated with excessive  $\beta_1AR$  activation.

#### Introduction

43

44

45

46

47

48

49

50

51

52

53

54

55

56

57

58

59

G protein-coupled receptors (GPCRs) are integral regulators of cellular signaling in both health and disease and are readily modulated by an array of molecular modalities, including small molecules, peptides, and hormones (1, 2). Accordingly, GPCRs serve as exemplary therapeutic targets as they are highly amenable to pharmacological modulation and currently comprise more than 30% of all biological entities targeted by FDA-approved drugs (3). As fundamental mediators of the chronotropic and inotropic response in the heart, the  $\beta$ -adrenergic receptor ( $\beta$ AR) subfamily of GPCRs remains one of the most extensively pursued cardiovascular disease targets. βARs are activated via binding of the catecholamine hormone epinephrine and the neurotransmitter norepinephrine to the orthosteric (i.e., endogenous) ligand binding site on the extracellular surface of the receptor. In turn, signaling cascades mediated by heterotrimeric G<sub>s</sub> and/or β-arrestin transducer proteins are initiated to positively regulate heart rate and contractile dynamics (4). While acute stimulation of  $\beta$ ARs, particularly via the more abundantly expressed cardiac  $\beta_1$ AR subtype, is an essential physiological response to support increased cardiovascular demand, chronic catecholamine signaling is exceedingly damaging to the heart and is associated with maladaptive morphological remodeling, cardiomyocyte apoptosis, fibrosis, lethal arrhythmias, and heart failure (4).

60

61

62

63

64

65

For decades, traditional orthosteric  $\beta$ -blockers, which competitively antagonize the endogenous ligand binding site of  $\beta$ ARs, have been widely used to combat pathological  $\beta_1$ AR over-activation. While  $\beta$ -blockers are highly efficacious in reducing morbidity and mortality in heart failure (5), their use is often complicated by adverse effects such as hypotension, fatigue, and reduced exercise capacity that are often associated with the nonselective inhibition of other  $\beta$ AR

subtypes, such as the  $\beta_2ARs$  expressed in vascular and respiratory tissues. These limitations are particularly pertinent to the treatment of catecholaminergic polymorphic ventricular tachycardia (CPVT), a disease characterized by extreme susceptibility to lethal ventricular tachyarrhythmia that develops in direct response to catecholamines (6). To date, nonselective  $\beta$ -blockers such as nadolol and propranolol are the most effective front-line therapy for CPVT (7). However, achieving a maximally tolerated dose without major adverse effects or the occurrence of breakthrough arrhythmias remains a major challenge (5, 8). Thus, CPVT, among other cardiac disorders, could highly benefit from the discovery of efficacious  $\beta$ AR ligands with improved subtype selectivity for the  $\beta_1$ AR.

While most GPCR-targeting drugs, including β-blockers, bind the orthosteric site, a rapidly expanding approach to identify ligands with enhanced specificity, efficacy, and modulatory function is to target allosteric sites of the receptor (9, 10). Allosteric modulators bind to regions that are topographically distinct from the endogenous ligand binding pocket and can increase (positive allosteric modulator, PAM) or suppress (negative allosteric modulator, NAM) the activity of receptors stimulated by an orthosteric ligand. Given that allosteric sites of receptors are more prone to evolutionary divergence and thereby more structurally diverse compared to the orthosteric region that is often highly conserved amongst closely related receptors of the same family, allosteric modulators are more likely to be subtype-selective with less potential for off-target effects. Moreover, allosteric modulators typically do not possess robust intrinsic activity of their own since they do not directly bind the orthosteric site and should exert a minimal effect on receptor function in the absence of an orthosteric ligand, potentially enabling increased tolerance at higher doses. Also supporting their potential tolerability is the "ceiling effect", which refers to

the saturation of allosteric effects once all binding sites are occupied (11). Together, these properties of allosteric modulators highlight their potential therapeutic advantages relative to their classical orthosteric counterparts (9, 10).

We therefore conducted a DNA-encoded small molecule library (DEL) screen to identify allosteric modulators of the  $\beta_1AR$  possessing functional antagonism for use as a therapeutic molecule for treating cardiac diseases. DEL screening is a powerful high-throughput drug discovery technique that enables the simultaneous evaluation of large and chemically diverse libraries where individual molecules are covalently linked to a unique DNA tag. Following multiple iterative rounds of affinity selection screening >1 billion unique small molecules comprising the OpenDEL<sup>TM</sup> library (HitGen Inc.) against purified, functional,  $\beta_1ARs$  reconstituted in lipid nanodiscs, we performed a chemical feature enrichment analysis and discovered Compound 11 (C11) as a highly selective allosteric modulator of the  $\beta_1AR$ . Here, we demonstrate the unique pharmacological and functional properties of C11 for modulating  $\beta_1AR$ -mediated signaling and show its therapeutic potential for the treatment of CPVT.

#### Results

106

107

108

109

110

111

112

113

114

115

116

117

118

119

120

121

122

123

# Discovery of Compound 11 (C11) through DNA-encoded small molecule library screening

To discover allosteric modulators of the β<sub>1</sub>AR with pharmacological and functional properties suitable for potential use as a therapeutic, we conducted a DEL screen using purified β<sub>1</sub>ARs reconstituted in lipid nanodiscs (also known as high-density lipoprotein, HDL particles) mimicking the native membrane environment (12). To enable the discovery of molecules that target unique β<sub>1</sub>AR conformational states, we screened five different conditions: β<sub>1</sub>AR bound to the high-affinity agonist BI-167107 (BI), BI-bound β<sub>1</sub>AR in complex with either heterotrimeric G<sub>s</sub> or  $\beta$ -arrestin1, and the empty nanodisc and un-liganded  $\beta_1AR$  (apo- $\beta_1AR$ ) controls (Fig 1A). Chimeric β<sub>1</sub>ARs harboring the phosphorylated C-terminal tail of the V<sub>2</sub>R (β<sub>1</sub>V<sub>2</sub>Rpp) were engineered to convert β<sub>1</sub>AR to a Class B GPCR, thereby strengthening β-arrestin1 complex stability (13) (SFig. 1A-B). Transducer complexes were further reinforced via conformation stabilizing nanobodies (Nbs) or antibody fragments (Fabs) including Nb35, Nb25, and Fab30 (Fig. 1A). Fab30 and Nb25 specifically bind and stabilize the active state of β-arrestin1, while Nb25 enhances the stability of the G-protein-bound receptor complex (14-16). Prior to the screen, nanodiscs were functionally validated via radioligand binding (SFig. 1C-D) and the affinity selection protocol was optimized as described in Supplemental Materials and Methods and Supplemental Figure 2.

124

125

126

127

128

To facilitate the isolation of small molecule  $\beta_1AR$  binders from the >1 billion unique compounds comprising the OpenDEL<sup>TM</sup> library, nanodisc  $\beta_1AR$  complexes were immobilized to neutravidin beads via biotinylation of the nanodisc membrane scaffold protein, MSPD1E3 (Fig. 1B). Following two consecutive rounds of affinity selection, eluted molecules were purified, PCR

amplified, and subjected to high-throughput next-generation sequencing to decode binders (Fig. 1B). The decay of library molecules throughout each round of selection was monitored via qPCR using a universal primer set that amplifies all molecules in the library (Fig. 1C-D). In each experimental condition, approximately  $1x10^7$  molecules were collected in the final elution from the  $1x10^{15}$  molecules applied as input (Fig. 1C-D).

Putative hit molecules were identified via comprehensive bioinformatics analysis of the chemical structure similarities among molecules present in the decoded dataset. Enriched chemical features that aligned with our scenario of interest (i.e., an unbiased negative allosteric modulator) were evaluated based on their abundance (or absence) in a particular experimental condition. Using this filtering criteria, we discovered a family of compounds sharing a common partial structure (i.e., R2 and R3) that was significantly enriched in the BI-bound  $\beta_1AR$  and apo- $\beta_1AR$  conditions, minimally present in the  $G_s$  and  $\beta$ -arrestin1 samples, and completely absent in the empty nanodisc control (Fig. 1E-F). From this family, Compound C11 (C11) was selected for further characterization off-DNA based upon its enrichment profile and relatively high copy number in relation to other members of the compound family (Fig. 1E-G). We predicted that C11 possessed the greatest potential as a  $\beta_1AR$  negative allosteric modulator, a conclusion that was later corroborated through direct comparison with other structurally related compounds, as detailed below.

#### C11 potentiates the binding affinity of agonists and a subset of antagonists to the $\beta_1AR$

To interrogate the pharmacological properties of C11 on the  $\beta_1AR$ , we investigated the ability of C11 to modulate orthosteric ligand binding affinity via radioligand competition binding

experiments. Purified  $\beta_1AR$  nanodiscs were incubated with the radiolabeled  $\beta_1AR$  antagonist, <sup>125</sup>I-CYP, and serial concentrations of un-labeled orthosteric  $\beta_1AR$  agonists or antagonists. In the presence of C11, the binding affinity of norepinephrine, isoproterenol, dobutamine, and epinephrine for the  $\beta_1AR$  was significantly enhanced as evidenced by a ~0.4-log leftward shift and corresponding ~1.9-3-fold decrease in the IC<sub>50</sub> of the competition binding curve compared to vehicle control (Fig. 2A and C; Supplemental Table 1), demonstrating positive cooperativity between C11 and  $\beta_1AR$  agonists. Interestingly, C11 exhibited a probe-dependent effect with respect to orthosteric antagonist binding to the  $\beta_1AR$  since it potentiated the binding of a subset of antagonists or biased ligands (i.e., carvedilol, bucindolol, and alprenolol; up to 0.5-log leftward shift and ~3-fold IC<sub>50</sub> decrease) without affecting atenolol, metoprolol, or carazolol binding affinity (Fig. 2B-C; Supplemental Table 1). This indicates that the effect of C11 on orthosteric ligand binding to the  $\beta_1AR$  is specific to the ligand bound. Overall, these binding results are consistent with our screening output in which C11 was enriched in not only the inactive apo- $\beta_1AR$  state but also in BI-occupied active  $\beta_1AR$  condition.

To estimate the affinity of C11 for the  $\beta_1AR$ , the C11-mediated concentration-dependent increase in isoproterenol binding to the receptor (quantified as  $\Delta IC_{50}$  of the competition binding curve) was plotted as a function of increasing concentrations of C11 (SFig. 3A-C). The resulting LogEC<sub>50</sub> (-6.12, ~0.76 uM) derived from the non-linear fit suggests sub-micromolar binding affinity between C11 and the  $\beta_1AR$  in the presence of isoproterenol (SFig. 3A-C). In agreement with this, direct assessment of the physical interaction and binding affinity between C11 and active  $\beta_1AR$  bound to high-affinity agonist BI by isothermal titration calorimetry (ITC) revealed a dissociation constant (K<sub>D</sub>) of 4.75  $\mu$ M (SFig. 3D).

#### 

# C11 suppresses G protein and β-arrestin signaling downstream of agonist-activated β<sub>1</sub>AR

Given the positive cooperativity between C11 and orthosteric agonist binding to the  $\beta_1AR$ , we anticipated that C11 would enhance  $\beta_1AR$  downstream signaling functioning as a PAM. The functional impact of C11 on G protein and  $\beta$ -arrestin signaling in response to  $\beta_1AR$  activation was assessed via BRET-based and/or luciferase-based cellular signaling assays. To measure dissociation of  $G\alpha_s\beta\gamma$  upon  $\beta_1AR$  stimulation, HEK293T cells transiently overexpressing  $\beta_1AR$  with TRUPATH biosensor proteins  $G\alpha_s$ -RLuc8,  $G\beta_3$ , and  $G\gamma_9$ -GFP (17) were pre-treated with vehicle (DMSO) or 30  $\mu$ M C11 and stimulated with serial concentrations of isoproterenol (Fig. 3A). Surprisingly, despite its positive cooperativity with agonist binding, C11 substantially reduced maximal G protein dissociation (Fig. 3B-C) evidenced by an attenuation of the BRET signal decay. To measure  $G\alpha_s$ -mediated signaling downstream of agonist-activated  $\beta_1ARs$ , we quantified intracellular cAMP generation utilizing the luciferase-based GloSensor<sup>TM</sup> cAMP biosensor (Fig. 3D). Consistent with our TRUPATH results, pre-treatment with C11 significantly diminished maximal cAMP generation compared to vehicle-treated cells (Fig. 3E-F).

Utilizing similar BRET-based approaches, we evaluated the effect of C11 on the various functions of  $\beta$ -arrestin. To measure  $\beta$ -arrestin recruitment to agonist-activated  $\beta_1AR$ , we developed a BRET sensor pair consisting of  $\beta$ -arrestin2-GFP and a chimeric  $\beta_1AR$  containing the C-terminal tail of the V<sub>2</sub>R ( $\beta_1V_2R$ ) conjugated to RLucII (Fig. 3G; Supplemental Table 2) that was utilized to enhance  $\beta$ -arrestin affinity to agonist occupied  $\beta_1ARs$ . To measure  $\beta$ -arrestin-mediated receptor internalization,  $\beta_1V_2R$  was co-expressed with  $\beta$ -arrestin2-RLucII and the early endosomal marker FYVE-rGFP (18) (Fig. 3J). Strikingly, pre-treatment with C11 induced a robust decrease in both

β-arrestin recruitment to  $β_1V_2R$  (Fig. 3H-I), and β-arrestin-mediated receptor internalization into endosomes (Fig. 3K-L). These findings indicate that C11 acts as an unbiased functional NAM of agonist-activated  $β_1AR$  since it potently inhibits both Gs and β-arrestin signaling.

Given that ERK is one of the major cellular effectors of both Gs and  $\beta$ -arrestin signaling cascades, we next evaluated the effect of C11 on  $\beta_1AR$ -mediated ERK phosphorylation via immunoblotting. Consistent with our BRET-based assays, HEK293T cells transiently overexpressing  $\beta_1AR$  displayed a dose-dependent increase in ERK phosphorylation in response to serial concentrations of isoproterenol that was suppressed in cells pre-treated with C11 (Fig. 4A-C). Notably, ERK phosphorylation stimulated by carvedilol, a  $\beta$ -arrestin biased  $\beta AR$  ligand that has been previously shown to promote ERK phosphorylation in a  $\beta$ -arrestin dependent manner (19-22), was also attenuated in the presence of C11 (Fig. 4D-F). This indicates that C11 serves as a functional NAM of the  $\beta_1AR$  irrespective of the nature of the orthosteric ligand (i.e., full agonists versus biased ligands).

Taken together, in striking opposition to the positive cooperativity of agonist binding, our cellular signaling assays revealed that C11 is a potent inhibitor of  $\beta_1AR$ -mediated  $G\alpha_s$  and  $\beta$ -arrestin signaling. Moreover, its suppression of maximal  $\beta_1AR$  signaling efficacy reflects the classical pattern of non-competitive inhibition as would be expected from an allosteric modulator. With such a unique pharmacological and functional profile, our studies indicate that C11 likely belongs to a recently established class of allosteric modulators termed PAM-antagonists that potentiate agonist affinity for receptors while antagonizing downstream signaling (23). While

largely under-characterized to date, PAM antagonists are predicted to be especially favorable therapeutically due to their positive cooperativity on agonist binding affinity (23).

# The PAM-antagonist function of C11 is highly selective for $\beta_1ARs$

We next evaluated the pharmacological selectivity of C11 for the  $\beta_1AR$  by interrogating its effect on orthosteric ligand binding to the  $\beta_2AR$  subtype. Radioligand binding experiments utilizing  $\beta_2AR$  nanodiscs demonstrated that C11 did not significantly alter the isoproterenol binding curve compared to vehicle, whereas carvedilol binding to the  $\beta_2AR$  is potentiated by  $\sim 2.6$ -fold ( $\sim 0.4$ -log leftward shift) in the presence of C11 (Fig. 5A-C). These data indicate that C11 also binds and modulates ligand binding to the  $\beta_2AR$ , given that it potentiates carvedilol binding to both subtypes, but does not elicit an increase in affinity between  $\beta_2AR$  and the agonist isoproterenol. Of note, this  $\beta AR$  subtype-dependent activity is reminiscent of the recently discovered  $\beta_2AR$  positive allosteric modulator, Compound 6, that potentiates carvedilol binding to both  $\beta_1AR$  and  $\beta_2AR$  while selectively increasing agonist binding to the  $\beta_2AR$  only (22, 24, 25).

To determine the functional selectivity of C11 for the  $\beta_1AR$ , we performed various counter assays interrogating G protein and  $\beta$ -arrestin signaling stimulated by alternative GPCRs of the cardiovascular system including the  $\beta_2AR$ , AT1R, and M3R. Importantly, C11 did not significantly impact G protein dissociation or  $\beta$ -arrestin internalization downstream of either agonist-activated  $\beta_2AR$  (Fig. 5D-G) or AT1R (Fig. 5H-K). Moreover, C11 had no effect on intracellular Ca<sup>2+</sup> release downstream of carbachol-activated endogenous M3R (Fig. 5L-N). Together, these experiments indicate that the functional effects of C11 are highly selective for the  $\beta_1AR$  subtype.

#### 243

244

245

246

247

248

249

250

251

252

253

254

255

256

257

258

259

260

261

262

263

264

# C11 is a superior PAM antagonist relative to structurally related OpenDEL<sup>TM</sup> analogs.

To gain mechanistic insights into the chemical features that support the pharmacological and functional effects of C11 on the  $\beta_1AR$  and to evaluate whether small chemical modifications in its structure would confer altered efficacy as a PAM antagonist, we characterized a panel of C11 analogs C11-A through C11-I (SFig. 4) and evaluated their effects on ligand binding and β<sub>1</sub>ARmediated signaling. These analogs comprise additional members of the enriched family of structurally related OpenDEL<sup>TM</sup> molecules detected via our bioinformatics analysis (Fig. 1E-F; C11-A through F and H) as well as several truncated derivatives (C11-G and I). The ability of C11 to potentiate agonist and antagonist binding to the  $\beta_1AR$  was largely unaffected by modifying the R1 chemical group, given the lack of substantial differences in the IC<sub>50</sub> shifts between C11 and analogs A-F and H (SFig. 5A-C). Remarkably, truncation of the extended hydrocarbon chain comprising the R3 chemical group in C11 and C11-H (generating C11-G and C11-I, respectively) resulted in complete loss of the positive cooperativity of isoproterenol and carvedilol binding to the  $\beta_1AR$  (SFig. 5A-C). These results are corroborated by evaluation of  $G\alpha_s$  dissociation and  $\beta$ arrestin recruitment to the β<sub>1</sub>AR via BRET, wherein the R3-truncated C11-G and C11-I analogs completely lose the antagonistic functions of C11 (SFig. 5D-F) while the remaining analogs that vary in the R1 group remain functional antagonists to a similar or lesser extent than C11 (SFig. 5D-F). Together, these data demonstrate that the identity of the R1 chemical group is largely exchangeable, while the R3 extended hydrocarbon chain is critical for its function and engagement with the receptor. These findings provide several mechanistic insights into the precise chemical features that mediate the activity of C11 and indicate that C11 is a superior PAM antagonist relative

to a panel of structurally related molecules selected from the OpenDEL<sup>TM</sup> library. Lastly, C11-G, the R3-truncated form of C11, was revealed as a complete 'loss-of-function' analog.

267

268

269

270

271

272

273

274

275

276

277

278

279

280

281

282

283

284

285

286

265

266

# C11 reduces basal contractility and suppresses the isoproterenol response in isolated wildtype cardiomyocytes

Following our comprehensive pharmacological and cellular characterizations, we investigated the impact of C11 on cardiac signaling and function in primary cardiomyocytes expressing endogenous levels of the β<sub>1</sub>AR. Ventricular cardiomyocytes isolated from adult wildtype mice were pre-treated with DMSO or serial concentrations of C11 and paced at 1 Hz. Pretreatment with 30 µM C11 induced a significant reduction in basal fractional shortening compared to cells pre-treated with DMSO (Fig. 6A-B; Supplemental Table 3). To evaluate whether this inhibitory effect was specific to C11 and not a non-selective consequence of its high-dosage (up to 30 μM), we employed the loss-of-function analog, C11-G, that does not modulate β<sub>1</sub>ARmediated signaling (SFig. 5A-F). Here, pre-treatment with 30 µM C11-G did not affect basal contractility in wild-type cardiomyocytes compared to vehicle control suggesting a direct effect of C11 on cardiomyocyte contractility (Fig. 6A-B; Supplemental Table 3). To assess whether the C11-mediated reduction in basal contractility results from direct modulation of the  $\beta_1AR$ , we pretreated ventricular cardiomyocytes isolated from β<sub>1</sub>AR<sup>-/-</sup> mice with DMSO or serial concentrations of C11. Importantly, 10 µM C11 showed little effect on basal contractility while 30 µM C11 also elicited a significant reduction in basal contractility in  $\beta_1AR^{-/-}$  cardiomyocytes (Fig. 6C), albeit to a lesser extent than in wild-type (Fig. 6A-B). These data suggest that the C11-mediated suppression of basal contractility at high concentrations (i.e., 30 µM C11) is due to partial offtarget effects, while 10  $\mu$ M C11 shows little off-target effect. We therefore selected 10  $\mu$ M C11 for subsequent functional and signaling assays in isolated cardiomyocytes.

To determine the effect of C11 on the isoproterenol-induced contractile response, we stimulated isolated wild-type cardiomyocytes with serial concentrations of isoproterenol in the presence or absence of 10  $\mu$ M C11. In line with its ability to suppress G $\alpha_s$  and  $\beta$ -arrestin signaling downstream of agonist-activated  $\beta_1$ AR, C11 substantially suppressed the dose-dependent increase in fractional shortening and contractile kinetics mediated by isoproterenol (Fig. 6D-G). To corroborate this finding biochemically, we selected representative Ca<sup>2+</sup> cycling or sarcomeric cellular effectors of  $\beta_1$ AR activation, namely phospholamban (PLN) and troponin I (TnI), and assessed their phosphorylation status in isolated cardiomyocytes in the presence of isoproterenol via immunoblotting. Pre-treating wild-type cardiomyocytes with 10  $\mu$ M C11 robustly suppressed the isoproterenol-induced phosphorylation of PLN and TnI at the canonical protein kinase A (PKA) phosphorylation sites (pPLN Ser16 and pTnI Ser23/24) as well as Thr17 mediated by Ca<sup>2+</sup>/calmodulin protein kinase II (CaMKII) on PLN (Fig. 6H-I), providing further evidence of C11's ability to block  $\beta_1$ AR-mediated signaling in the heart.

# C11 restores regular contractile rhythm and suppresses spontaneous Ca<sup>2+</sup> release in CSQ2<sup>-</sup> cardiomyocytes

Given the robust inhibition of the isoproterenol response in cardiomyocytes pre-treated with C11, we next evaluated its potential as a therapeutic molecule for CPVT utilizing cardiomyocytes from mice that are constitutively null for CSQ2 (26). Previous studies have demonstrated that CSQ2<sup>-/-</sup> mice are highly susceptible to catecholamine-induced arrhythmia in the

form of frequent premature ventricular contractions (PVCs), increased heart rate variability, and increased diastolic Ca<sup>2+</sup> leak due to spontaneous Ca<sup>2+</sup> release events (26). Consistent with this, isolated ventricular cardiomyocytes from CSQ2<sup>-/-</sup> mice developed an arrhythmic-like phenotype when stimulated with isoproterenol during 1 Hz pacing, evidenced by a robust increase in both the frequency of contractions and the variability in the time interval between consecutive beats that is reminiscent of the irregular contractile rhythms observed in vivo (Fig. 7A) (26). Remarkably, pretreatment with 10 µM C11 completely attenuated isoproterenol-mediated spontaneous cellular beating and restored regular contractile frequency in CSO2<sup>-/-</sup> cardiomyocytes (Fig. 7A-E). To further corroborate the protective effect of C11 in CSO2-/- cardiomyocytes, we measured spontaneous Ca<sup>2+</sup> release events elicited by isoproterenol immediately following termination of 0.5 Hz pacing. In line with the blockade of isoproterenol-induced spontaneous contractile activity in CSO2-/- cardiomyocytes (Fig. 7A-E), pre-treatment with 10 µM C11 also prevented the development of spontaneous Ca<sup>2+</sup> release events following isoproterenol stimulation (Fig. 7F-J). Of note,  $10~\mu M$  C11 had no significant effect on the amplitude or kinetics of paced Ca<sup>2+</sup> transients in CSQ2-/- cardiomyocytes (SFig 6A-E), nor did it affect caffeine-induced Ca<sup>2+</sup> release in wildtype cells (SFig 7A-B), indicating that C11 has no direct impact on baseline Ca<sup>2+</sup> signaling.

326

327

328

329

330

331

332

310

311

312

313

314

315

316

317

318

319

320

321

322

323

324

325

#### C11 suppresses exercise-induced ventricular tachycardia in vivo

Intense exercise stress is the principal trigger for ventricular tachycardia (VT) and sudden cardiac death in individuals with CPVT. To investigate the therapeutic potential of C11 in a physiologically relevant setting, we recorded cardiac electrical activity via telemetry in conscious, non-anesthetized, CSQ2<sup>-/-</sup> mice subjected to graded treadmill exercise designed to mimic strenuous physical exertion in humans (Fig. 8A-C). To determine an appropriate dosing regimen for C11,

we first confirmed that the compound is stable long-term (up to 72 hours) in vehicle solution at 37 °C via HPLC/MS (SFig. 8A). We also obtained the pharmacokinetic profile of C11 following intraperitoneal injection (10 mg/kg) and determined that C11 is detectable in plasma and heart at the highest level between 45 minutes to 1-hour post-injection (SFig. 8B). After surgical implantation of the telemetry module in the peritoneal cavity, mice were allowed a 3-day recovery period followed by 3-day acclimation phase during which they were conditioned to treadmill running (Fig. 8A). Guided by our pharmacokinetic findings, treadmill-acclimated CSQ2-/- mice were pre-treated for 45 minutes with either vehicle solution or 10 mg/kg C11 and subjected to forced treadmill running where workload (i.e. speed and incline) was periodically increased over 30 minutes (Fig. 8B). Individual mice were delivered alternating treatments of vehicle or C11 four days apart (day 7 and 11, respectively; Fig. 8A) and thus each mouse served as its own internal control. To ensure robust analysis of C11's efficacy, mice lacking exercise-induced VT (i.e. less than 5 seconds) during vehicle treatment were not included for further study, limiting the assessment to animals with measurable baseline arrhythmogenic activity.

The total duration of sustained monomorphic and/or polymorphic VT defined as consecutive ectopic beats with unidirectional or bidirectional QRS waveforms, respectively (Fig. 8C), was quantified for each animal during graded exercise. Remarkably, the total duration of VT encompassing both monomorphic and polymorphic forms was significantly attenuated in C11-treated CSQ2<sup>-/-</sup> mice compared to when those same mice were pre-treated with vehicle solution (Fig. 8D). Given the variability in arrhythmic burden among vehicle-treated mice, we plotted the relative percent change in total VT duration for individual mice (Fig. 8E). This analysis revealed a median reduction in VT of approximately 50% following C11 treatment as compared to vehicle

(Fig. 8E). In addition to sustained episodes of VT, we assessed the incidence of premature ventricular contractions (PVCs) during the graded exercise test (SFig. 9A). While most individual mice also developed a reduction in PVCs following C11 treatment, this difference did not reach statistical significance (p=0.195, Wilcoxon matched pairs signed rank test; SFig. 9B-C). This may be attributed to the significant role catecholamines have in inducing and propagating sustained VT as compared to isolated PVC events.

We further tested the ability of C11 to suppress arrhythmic events in comparison to nadolol, an orthosteric β-blocker that remains the most efficacious and widely used pharmacological therapy for CPVT. To identify a dose of nadolol that elicited a mild but not complete reduction in heart rate in response to exercise, we sequentially treated individual wild-type mice with vehicle, 0.005, 0.01, and 0.1 mg/kg in a repeated measures design (Supplementary Fig. 10). Given that treatment with 0.1 mg/kg nadolol markedly suppressed the heart rate response to exercise and may represent a level of drug that is likely to cause symptomatic side effects, we selected 0.01 mg/kg as a low-dose nadolol condition to be tested in combination with C11. We subsequently delivered vehicle, low-dose nadolol (0.01 mg/kg), low-dose nadolol (0.01 mg/kg) in combination with C11 (10 mg/kg), or C11 alone (10 mg/kg) to individual CSQ2<sup>-/-</sup> mice with a 7-day washout period between treatments (Fig. 8A) and quantified VT duration during exercise. Treatment with C11in combination with low-dose nadolol significantly reduced the duration of exercise-induced VT compared to low-dose nadolol alone and to a similar extent as C11 alone (Fig. 8F-G).

Taken together, these results demonstrate the therapeutic capability of C11 in mitigating exercise induced arrhythmias associated with the pathological over-activation of  $\beta_1AR$  in the heart and underscore its potential as a new class of drug to block the  $\beta_1AR$  in disease states.

#### Discussion

Herein, we report the discovery of the β<sub>1</sub>AR-selective allosteric modulator, C11 (and its analog molecules), via DEL screening and comprehensively interrogate its unique pharmacological properties, functional effects, and therapeutic applications in the heart. Our studies reveal that C11 binds to the β<sub>1</sub>AR with low-micromolar affinity and potentiates the binding of agonists and a subset of antagonists to the β<sub>1</sub>AR in a subtype-specific fashion. In contrast to its positive cooperativity with orthosteric agonists, C11 potently decreases agonist-activated β<sub>1</sub>AR signaling, suppresses the isoproterenol response in isolated cardiomyocytes, and largely prevents the development of spontaneous contractile and Ca<sup>2+</sup>release events in a model of CPVT. Most importantly, treatment with C11 significantly mitigates exercise-induced ventricular tachycardia in CPVT mice. C11 therefore represents a promising therapeutic molecule for the treatment of cardiac disease, illustrated herein in the context of CPVT.

CPVT is an inherited arrhythmic disorder characterized by the heightened susceptibility to catecholamine-induced polymorphic or bidirectional ventricular tachycardia initiated by exercise or emotional stress in the absence of structural heart disease (6). The genetic basis is commonly associated with mutations in proteins of the sarcoplasmic reticulum (SR) Ca<sup>2+</sup> release complex (i.e., RyR2 or CSQ2), leading to SR Ca<sup>2+</sup> overload, spontaneous Ca<sup>2+</sup> release due to hyperactive RyR2, and arrhythmogenic Ca<sup>2+</sup>-induced delayed after depolarizations potentially culminating in sudden cardiac death (6, 27). CPVT is a severe life-threatening disorder with mortality rates ranging from 30-50% in untreated patients by the age of 40 (28). β-blockers such as nadolol are currently the most efficacious therapy for CPVT and have been successful in decreasing arrhythmic risk and severity (7, 29). However, β-blockers are not completely effective as recurrent

arrhythmic events occur in up to 37.2% of treated patients, with 15.3% being near-fatal and 6.4% fatal during an 8-year follow up period after beginning treatment (30). A major obstacle that remains is achieving a maximally tolerated dose of β-blocker due to adverse effects in vascular tissues (i.e., hypotension) where the β<sub>2</sub>AR is highly expressed (5, 8). Moreover, cardio-selective βAR antagonism would be especially optimal in the presence of respiratory disorders such as asthma or COPD. As a β<sub>1</sub>AR-selective allosteric modulator, C11 should maximize its inhibitory effects once all allosteric sites are occupied (i.e. the ceiling effect) and therefore has the potential to be used at a therapeutically effective dose with minimal off-target concerns (11). Beyond this, PAM antagonism may confer additional therapeutic benefits that are elaborated further below.

While we currently demonstrate the therapeutic potential of C11 utilizing a model of CPVT where the primary pathological mechanism is directly related to  $\beta_1AR$  activation, C11 could be applied as a treatment for a wide range of cardiac diseases (i.e., hypertrophic and dilated cardiomyopathy) or arrhythmic disorders (i.e., long QT syndrome, arrhythmogenic cardiomyopathy, atrial fibrillation) that are potentiated by excessive sympathetic stimulation and where  $\beta$ -blockers have been previously shown to be beneficial (7). It is also interesting to speculate that C11 could possibly modulate the activity of  $\beta_1AR$ -activating autoantibodies that develop during chronic heart failure (31-33), and in conditions where enhanced sympathetic activity results in high synaptic catecholamine release such as exertional angina and postural orthostatic tachycardia syndrome. An important consideration in the clinical use of C11 would be the probe dependence of its modulatory effects on distinct orthosteric  $\beta$ -blockers. Our studies showed that C11 potentiates the affinity of a subset of antagonists to the  $\beta_1AR$  such as the  $\beta$ -arrestin-biased ligand carvedilol and suppresses carvedilol-mediated ERK activation. It remains to be determined

whether C11 also diminishes the antagonist function of carvedilol on G protein signaling or whether C11 potentiates the inhibition. Further clarifying the pharmacological properties of C11 will be essential for assessing whether it could potentially be used in combination with orthosteric β-blockers, such as carvedilol, to enhance their efficacy. Our evaluation of the therapeutic effectiveness of C11 when used in combination with low-dose nadolol, however, implies that physiologically it may enhance the inhibitory function of certain orthosteric antagonists.

The unique pharmacological and functional profile exhibited by C11 shows features similar to a recently recognized subclass of allosteric modulators termed PAM-antagonists that increase the binding affinity for receptors but decrease the functional efficacy of the agonist (23). There are several major advantages to this mechanism of signaling blockade relative to traditional orthosteric antagonists like  $\beta$ -blockers. Specifically, in contrast to orthosteric antagonists and even canonical NAMs that act competitively with the agonist by favoring an inactive receptor conformation, the potency and efficacy of a PAM-antagonist is actually *potentiated* in the presence of increasing agonist concentration due to their positive cooperativity on agonist binding. Moreover, PAM-antagonists such as C11 are further advantageous in that they have a higher propensity to bind agonist-bound receptors, thereby preferentially targeting pre-existing pathological overactivation (23). Along with its selective effects on the  $\beta_1AR$ , the pharmacological properties conferred by PAM-antagonism underscore the potential advantageous therapeutic properties of C11 over canonical non-selective orthosteric  $\beta$ -blockers.

While C11 has shown reciprocal effects on agonist binding affinity and functional efficacy, the precise inhibitory mechanism, binding site, and receptor conformation it promotes remain

outstanding questions. To date, only several PAM-antagonists are currently described, and their mechanism of action is largely elusive. The first reported PAM-antagonist, ifenprodil, was discovered in 1996 as a neuroprotective modulator of the N-methyl-D-aspartate (NMDA) glutamate receptor ion channel (34). In the following decades, PAM-antagonists targeting the free fatty acid 3 (FFA-3) receptor (35) and the cannabinoid 1 (CB1) receptor (36, 37) were identified. Previous studies utilizing site-directed fluorescent labeling characterizing the CB1 PAMantagonist, Org27569, have reported that Org27569 blocks conformational changes associated with G protein binding suggesting that it locks the CB1 receptor in an agonist-bound, nonsignaling, early-activation intermediate state (38). Alternative hypotheses regarding the mechanism of PAM-antagonists include stabilizing a non-signaling quaternary complex comprised of receptor, agonist, modulator, and transducer, or perhaps steric blockade of transducer binding. Signaling bias should also be considered, as some PAM antagonists could have selective effects on specific pathways like SBI-553, a β-arrestin-biased PAM of the neurotensin receptor 1 (NTSR1) that selectively suppresses  $G\alpha q$  signaling while potentiating  $\beta$ -arrestin signaling through promoting a β-arrestin-selective receptor conformation (39, 40). While we have generated some preliminary structure-activity insights of C11 via characterizing a panel of analogs, future biophysical and structural studies will be required to precisely determine the binding location and mechanism of action of C11.

465

466

467

468

469

447

448

449

450

451

452

453

454

455

456

457

458

459

460

461

462

463

464

Through a DEL screen utilizing the OpenDEL<sup>TM</sup> small molecule library (HitGen Inc.) comprising over 1 billion unique compounds, we discovered a subtype-selective PAM-antagonist allosteric modulator of the  $\beta_1AR$ . Given its unique pharmacological and functional profile and demonstrated efficacy in suppressing pathological contractile and electrophysiological events in

experimental CPVT, C11 is a promising therapeutic candidate that holds great potential to be developed as a drug for a wide range of heart diseases that have as its pathological basis susceptibility to high catecholamine states.

473

#### **Materials and Methods:**

Sex as a biological variable

Experiments evaluating the therapeutic potential of C11 in suppressing exercise-induced VT were conducted using male CSQ2<sup>-/-</sup> mice. Female CSQ2<sup>-/-</sup> mice did not exhibit measurable baseline arrhythmogenic activity during exercise. Therefore, female CSQ2<sup>-/-</sup> mice were not included in the final analysis. Given these apparent sex-differences inherent to the CSQ2<sup>-/-</sup> phenotype, the efficacy of C11 *in vivo* was evaluated using male mice only.

#### Radioligand competition binding

Radioligand competition binding experiments were performed as previously described (22). Briefly, purified  $\beta_1AR$ ,  $\beta_1V_2Rpp$ , or  $\beta_2AR$  nanodiscs generated as described in the Supplemental Materials and Methods were incubated with 60 pM of the radiolabeled orthosteric antagonist, [I<sup>125</sup>]-cyanopindolol (I<sup>125</sup>CYP; 2200 Ci/mmol, PerkinElmer, Waltham, MA), and serial concentrations of unlabeled orthosteric ligand in binding buffer (20 mM HEPES pH 7.4, 100 mM NaCl) supplemented with 0.1% bovine serum albumin (BSA) and 1 mM ascorbic acid at room temperature for 2 hours to reach equilibrium. Non-specific binding was evaluated in the presence of 20  $\mu$ M propranolol. To validate nanodisc preparations, serial concentrations of purified heterotrimeric  $G_s$  (10-320 nM) or  $\beta$ -arrestin1-mc (0.1-1  $\mu$ M) were included in the binding reaction with  $\beta_1AR$  or  $\beta_1V_2Rpp$  nanodiscs, respectively, to confirm transducer cooperativity (SFig. 1C-D). To evaluate the effect of allosteric modulators on orthosteric ligand binding to  $\beta$ ARs, reactions included the indicated concentration of allosteric compound (0.05-30  $\mu$ M) or an equivalent volume of vehicle (0.19% DMSO). Equilibrated binding reactions were harvested by rapid filtration onto 0.3% polyethyleneimine (PEI)-soaked GF/B glass fiber filter paper (Brandel) and washed

extensively with ice-cold binding buffer.  $I^{125}$ -CYP was detected with the WIZARD<sup>2</sup> 2-detector Gamma Counter (PerkinElmer) and the raw counts per minute (cpm) were normalized to the percent of maximal  $I^{125}$ -CYP binding. The mean  $\pm$  SEM of at least 3 independent experiments performed in duplicate were plotted in GraphPad Prism and fit to a one-site binding model to retrieve  $IC_{50}$ . C11-mediated log shifts in the nonlinear fit are presented as  $\Delta IC_{50}$  (Vehicle – C11) and statistical analysis was performed using a paired two-tailed t-test of raw  $IC_{50}$  values (Supplemental Table 1). Statistical comparisons of the  $\Delta IC_{50}$  between C11 and its analogs (C11A-I) were conducted by one-way ANOVA with Dunnett's post-hoc test (GraphPad Prism).

## *G protein dissociation assay (TRUPATH)*

G protein dissociation was evaluated by the BRET-based TRUPATH assay as originally described in (17) with minor modifications. Briefly, 2.25 x 10<sup>6</sup> HEK293T cells maintained in growth media were seeded in a 10 cm dish and incubated overnight. On the next day, cells were transfected with 0.75 μg of human FLAG-β<sub>1</sub>AR (or FLAG-β<sub>2</sub>AR), with Gα<sub>8</sub>S-RLuc8, Gβ3, and Gγ9-GFP at a 1:1:1:1 DNA ratio. For AT1R counter assays, 0.75 μg of human FLAG-AT1R (41) was transfected along with 0.75 μg of Gα<sub>q</sub>-RLuc8, Gβ3, and Gγ9-GFP. After 24 hours, cells were trypsinized, resuspended in low-serum medium (1X MEM without phenol red, supplemented with 2% FBS, 1% HEPES, 1% anti-anti, 1% glutamine, and 1% P/S), and re-plated in a white, clear bottom 96-well assay plate at a density of 100,000 cells/well for overnight incubation. Prior to experimentation, low-serum media was aspirated and replaced with 1X Assay Buffer (Hank's Balanced Salt Solution, HBSS, supplemented with 20 mM HEPES) and incubated for 10 minutes at 37 °C. Cells were pre-treated with vehicle (0.19% DMSO) or 30 μM C11 prepared in 1X Assay Buffer for 20 minutes at 37 °C. To assess β<sub>1</sub>AR-mediated G protein dissociation, 100 nM ICI-

118,551 was included during pre-treatment to block activation of endogenous β<sub>2</sub>ARs. Cells were then stimulated with serial concentrations of isoproterenol for 10 minutes at 37 °C. BRET emission ratios (GFP/RLucII) were measured immediately following the addition of 5 μM coelenterazine 400a (Nanolight Technology, Norman, OK) on a Biotek Neo2 microplate reader (Agilent Technologies, Santa Clara, CA) using the 410 nm (donor) and 515 nm (acceptor) filter pair. At least three independent experiments performed in duplicate were fitted to a log(agonist) vs response (three parameter) model in GraphPad Prism and baseline subtracted to assess net BRET ratio. Statistical analysis of the nonlinear curve fit (E<sub>max</sub>) was evaluated by two-tailed t-test.

#### GloSensor<sup>TM</sup> assay

The GloSensor<sup>TM</sup> assay (Promega) was performed as previously described with minor modifications (22). Briefly, 2.25 x  $10^6$  HEK293T cells maintained in growth media were seeded in a 10 cm plate and transfected 24 hours later with 25 ng of human FLAG- $\beta_1$ AR and 6  $\mu$ g of the GloSensor cAMP biosensor plasmid (Promega). On the following day, cells were re-plated into a white, clear bottom 96-well plate at a density of 50,000 cells/well in low-serum medium (1X MEM without phenol red, supplemented with 2% FBS, 1% HEPES, 1% anti-anti, 1% glutamine, and 1% P/S) and incubated overnight. Prior to experimentation, low-serum media was aspirated and replaced with the GloSensor<sup>TM</sup> reagent (2 mM; Promega) prepared in 1X Assay Buffer (HBSS with 20 mM HEPES) and incubated at room temperature for 1.5 hours. Cells were pre-treated with vehicle (0.19% DMSO) or 30  $\mu$ M C11 prepared in 1X Assay Buffer for 20 minutes at room temperature, along with 100 nM ICI-118,551 to block activation of endogenous  $\beta_2$ ARs. Cells were then stimulated with serial concentrations of isoproterenol for 5 minutes and luminescent values were recorded using the Biotek Neo2 microplate reader (Agilent Technologies). The mean  $\pm$  SEM

of at least three experimental replicates performed in duplicate were fit to a log(agonist) vs response (three parameter) model in GraphPad Prism and normalized to the percent of vehicle maximum. Statistical analysis of the nonlinear curve fit (E<sub>max</sub>) was evaluated by two-tailed t-test.

546

547

548

549

550

551

552

553

554

555

556

557

558

559

560

561

562

563

564

565

543

544

545

#### *BRET-based* $\beta$ -arrestin recruitment and receptor internalization assays

Evaluation of β-arrestin recruitment and internalization was performed using BRET-based biosensors. One day prior to transfection, 2.25 x 10<sup>6</sup> HEK293T cells maintained in growth media were seeded in a 10 cm dish. For  $\beta$ -arrestin recruitment assays, cells were co-transfected with 2 µg FLAG-β<sub>1</sub>V<sub>2</sub>R-RLucII and 1 μg β-arrestin2-eGFP (Addgene plasmid 35411; (42)), while β-arrestin internalization was evaluated via co-transfection of 2 μg FLAG-β<sub>1</sub>V<sub>2</sub>R (or FLAG-β<sub>2</sub>V<sub>2</sub>R or FLAG-AT1R for counter assays), with 1.5 μg β-arrestin2-RLucII, and 2.5 μg rGFP-FYVE (18). After 24 hours, cells were trypsinized, resuspended in low-serum medium (1X MEM without phenol red, supplemented with 2% FBS, 1% HEPES, 1% anti-anti, 1% glutamine, and 1% P/S), and re-plated at a density of 100,000 cells/well in a white, clear bottom 96-well plate for overnight incubation. Prior to experimentation, low-serum media was aspirated and replaced with 1X Assay Buffer (HBSS with 20 mM HEPES) and incubated for 10 minutes at 37 °C. Cells were pre-treated with vehicle (0.19% DMSO) or 30 μM C11 prepared in 1X Assay Buffer for 20 minutes at 37 °C. To evaluate BRET responses mediated by β<sub>1</sub>AR only, 100 nM ICI-118,551 was included during pre-treatment to block activation of endogenous β<sub>2</sub>ARs. Cells were then stimulated with serial concentrations of isoproterenol for 20 minutes (recruitment) or 25 minutes (internalization) at 37 °C. BRET emission ratios (GFP/RLucII) were measured immediately following the addition of 5 μM coelenterazine 400a (Nanolight Technology) on a Biotek Neo2 microplate reader (Agilent Technologies) using the 410 nm (donor) and 515 nm (acceptor) filter pair. At least three

independent experiments performed in duplicate were fitted to a log(agonist) vs response (three parameter) model in GraphPad Prism and baseline subtracted to assess net BRET ratio. Statistical analysis of the nonlinear curve fit ( $E_{max}$ ) was evaluated by two-tailed t-test.

# Cardiomyocyte isolation

Adult mouse ventricular cardiomyocytes were isolated using standard Langendorff perfusion procedures as previously described (43) from homozygous 12-16 week old C57BL/6J wild-type, β1AR knock-out (β1AR-/-) (44, 45), or calsequestrin 2 (CSQ2-/-) (26) mice. Mice were injected intraperitoneally with 200U of heparin and anesthetized under 3% isoflurane. Dissected whole hearts were placed immediately into perfusion buffer (120 mM NaCl, 14.8 mM KCl, 0.6 mM KH2PO4, 0.6 mM Na2HPO4, 1.2 mM MgSO4·7H20, 10 mM HEPES, 4.6 mM NaHCO3, 30 mM taurine, and 5.6 mM glucose, pH 7.3) and cannulated through the aorta. Hearts were perfused in retrograde for 3 minutes with oxygenated perfusion buffer and then for ~8 minutes with digestion buffer containing 2.4 mg/mL collagenase (Worthington) at 37 °C. To terminate enzymatic digestion, ventricular tissues were transferred to perfusion buffer containing 10% calf serum with 12.5 μM CaCl<sub>2</sub>. Myocytes were dissociated by trituration and gradually brought to physiological Ca<sup>2+</sup> (1.2 mM).

#### Contractility measurements

Cardiomyocytes isolated as described above were pre-treated with DMSO (0.3%) or C11 (3-30  $\mu$ M) for 20 minutes. Following pre-treatment, cells were stimulated with isoproterenol (0.01-1  $\mu$ M) or left un-treated (basal condition) and plated immediately in a FHD rotational cell chamber (Ionoptix, Westwood, MA) mounted on a Nikon Eclipse TE300 inverted microscope (40X 0.9 NA

objective, MRF00400, Nikon). Myocytes were paced at 1Hz (20V, MyoPacer, Ionoptix) and sarcomere length was recorded with IonWizard 7.2 using the MyoCam-S camera (Ionoptix). Ten consecutive contractions per cell were averaged for quantification of contractile magnitude and kinetics (IonWizard 7.2). At least 7-10 cells were quantified per experimental condition and averaged. Time intervals between consecutive contractions (i.e., peak-peak intervals) were measured during a representative five second recording in each cell. Interval variability plots were generated by plotting the peak-peak interval (n) against the peak-peak interval of the subsequent cellular contraction (n+1) for all cells in a particular treatment group. Only the myocytes that exhibited proper morphology (i.e., rod-shaped and striated) and were responsive to electrical stimulation were utilized for experimentation. Statistical comparisons between conditions were evaluated by one-way ANOVA with Tukey's post-hoc test.

### Phospho-PLN and phospho-TnI assay

Cardiomyocytes isolated as described above were pretreated with DMSO (0.3%) or 10 μM C11 for 20 minutes at room temperature prior to stimulation with 10 μM isoproterenol for 15 minutes while rotating. Cells were pelleted via centrifugation and homogenized in a 1:1 mixture of urea-thiourea lysis buffer (8 M urea, 2M thiourea, 3% SDS, 0.05 M tris-HCl, 0.03% bromophenol blue, 0.075 M DTT, pH 6.8) supplemented with protease and phosphatase inhibitors (Halt, Protease and Phosphatase Inhibitor Cocktail #78440, Thermo Fisher Scientific, Rockford IL) and 50% glycerol at 60 °C as described in (46). Lysates were separated on a 15% SDS-polyacrylamide gel and membranes were probed with the following primary antibodies: rabbit polyclonal antibodies targeting pPLN Ser16 (1:1000, 07-052, Millipore, Temecula, CA), pTnI Ser23/24 (1:1000, 4004S, Cell Signaling Technology, Danvers, MA), pPLN Thr17 (1:1000, Arigo

Biolaboratories, Taiwan) and TnI (1:1000, 4002S, Cell Signaling Technology), or mouse monoclonal antibodies to PLN (ab2865 Abcam, Cambridge, MA) with horseradish peroxidase (HRP)-conjugated secondary antibodies (1:3000; donkey anti-rabbit IgG, NA934V, and sheep anti-mouse IgG, NA931VS, Cytiva, Marlborough, MA). Densitometric analysis of phospho-PLN and phospho-TnI was performed with ImageJ and normalized to total PLN or TnI, respectively. Each experimental condition was performed in duplicate and averaged per biological replicate. Statistical analysis was performed with one-way ANOVA and Tukey's post-hoc test.

# *Cardiomyocyte Ca*<sup>2+</sup> *imaging*

To conduct live cell Ca<sup>2+</sup> imaging, ventricular myocytes isolated as described above were loaded with 10 μM CAL-520 (ab171868, Abcam) for 1 hour in 1X Ca<sup>2+</sup>-free Tyrode solution. Cells were then incubated with a 1:1 solution of RPMI/B27+ [RPMI 1640 (11875199, Thermofisher Scientific) with 2% B27 with insulin (17504044, Life Technologies)] and 1X Tyrode with 1.8mM CaCl<sub>2</sub> for 20 minutes prior to imaging. Cells were pretreated with DMSO (0.3%) or 10 μM C11 for 20 minutes and plated onto 200μg/ml laminin (L2020, Sigma-Aldrich) coated coverslips. Line scans were acquired on a Zeiss Laser Scanning Confocal 510 Meta Microscope (Carl Zeiss AG) at 0.1μm per pixel along the longitudinal axis of cardiomyocytes. Cells were paced at 0.5Hz with an IonOptix MyoPacer field stimulator (IonOptix) for ten seconds with a total imaging time of 34 seconds per cell. Fiji ImageJ v.1.53c (National Institutes of Health) was used to analyze Ca<sup>2+</sup> transients. Cells were scored as having sustained spontaneous calcium release events (SREs) if there were greater than 10 SREs less than 500ms apart. For caffeine-induced Ca<sup>2+</sup> transients, cells were paced at 0.5 Hz for 10 seconds and then treated with 10 mM caffeine (10

seconds after termination of pacing) on a Zeiss spinning disk Axio Observer.Z1 (40X, 215ms intervals). All Ca<sup>2+</sup> imaging experiments were performed at room temperature.

636

637

638

639

640

641

642

643

644

645

646

647

648

649

650

651

652

653

654

655

656

634

635

# Mouse graded treadmill exercise

Exercise experiments were performed with both young (8-12 weeks) and old (12 months) male CSQ2<sup>-/-</sup> mice. Genotypes were confirmed via PCR using previously described protocols (26, 44, 45, 47). CSQ2<sup>-/-</sup> mice were implanted with wireless ECG telemetry units (Model# ETA-F10, DSI-Harvard Bioscience, Inc.) and allowed to recover for 3 days. Female mice implanted with ECG telemeters were not used for these experiments since they did not show exercise-induced VT on repeated exercise testing. Pre-exercise conditioning involved acclimating mice to the rodent treadmill (Model: PanLab LE8708TS, Harvard Apparatus) for 30 mins/day on 3 consecutive days. On the first day of the acclimation period, mice were placed on a stationary treadmill belt and allowed to explore the treadmill chamber for 30 mins. On the subsequent two days of acclimation, the treadmill speed was set to 2 cm/s, 5 cm/s and 10 cm/s at a 25 ° incline for 10 mins at each speed. Acclimated mice were then subjected to a rigorous graded exercise protocol following a 45-minute pre-treatment with vehicle solution (10% dimethylacetamide, 40% PEG300, and 2% Tween80 in 48% saline) delivered intraperitoneally. The graded exercise protocol consisted of five stages where workload was incrementally increased every 5 minutes: 0 cm/s (baseline), 2 cm/s (light walking), 5 cm/s (fast walking), 10 cm/s (running), and 10 cm/s with a 25 ° incline (running) with increased difficulty), followed by a 5-minute recovery period at 0 cm/s. After 3 days of washout, mice were again subjected to the same graded exercise protocol following a 45-minute pre-treatment with 10 mg/kg C11 prepared in vehicle solution delivered intraperitoneally (Fig. 8A, upper panel).

For the nadolol dose-finding experiments, the graded treadmill stress test was performed repeatedly on individual wild-type mice with a 7-day washout period between sessions to ensure complete drug clearance before subsequent experiments. Heart rate was recorded during the prerunning baseline period (while positioned on the treadmill), as well as during walking (2 cm/s) and running (5 cm/s). For evaluation of low-dose nadolol prepared either alone or in combination with C11, drugs were administered intraperitoneally to CSQ2<sup>-/-</sup> mice with a 7-day washout period in between (Fig. 8A, lower panel).

To ensure the analysis was focused on CSQ2-- mice with measurable baseline arrhythmogenic activity, mice lacking exercise-induced VT (i.e. less than 5 seconds) during the vehicle-treated exercise run were not included in the study. Negative reinforcement with the shock grid set to 0.4 mV was used to encourage running. The treadmill experiments were conducted and reviewed with continuous data acquisition using Ponemah v6.6 software (DSI-Harvard Bioscience, Inc). The treadmill was disinfected with 70% ethanol after each session Monomorphic ventricular tachycardia was defined as four or more consecutive ventricular complexes with a consistent intrinsic shape, peak-to-peak interval, and amplitude. Polymorphic ventricular tachycardia was defined as ventricular complexes with progressive variations in intrinsic shape, peak-to-peak interval, or amplitude (48). Statistical comparisons of the duration of ventricular tachycardia and the total number of premature ventricular contractions (PVCs) were assessed by Wilcoxon matched pairs signed rank test or non-parametric repeated measures one-way ANOVA (Friedman's test).

Statistics

Statistical significance was determined by two-tailed t-test or one-way ANOVA with Tukey's post-hoc test for multiple comparisons (GraphPad Prism) unless indicated otherwise. Comparisons between the IC<sub>50</sub> of competition binding curves or the non-linear fit (Emax) of *in vitro* signaling assays were performed using an F-test (GraphPad Prism). Error bars represent mean  $\pm$  SEM. Sample sizes are indicated in the corresponding figure legends.

#### Study approval

All animal procedures were performed in accordance with NIH guidelines (Guide for the Care and Use of Laboratory Animals) and adhered to protocols approved by the Institutional Animal Care and Use Committee (IACUC) at Duke University Medical Center.

## Data availability

Data underlying each graph is reported in the Supporting Data Values file. Additional descriptions of the Materials and Methods, including sample sizes and statistical analyses, are included in the Supplemental Materials and corresponding Figure Legends.

#### 696 References

- 697 1. Pierce KL, Premont RT, and Lefkowitz RJ. Seven-transmembrane receptors. *Nat Rev Mol Cell Biol.* 2002;3(9):639-50.
- Rosenbaum DM, Rasmussen SG, and Kobilka BK. The structure and function of G-protein-coupled receptors. *Nature*. 2009;459(7245):356-63.
- 3. Sriram K, and Insel PA. G Protein-Coupled Receptors as Targets for Approved Drugs: How Many Targets and How Many Drugs? *Mol Pharmacol.* 2018;93(4):251-8.
- Grogan A, Lucero EY, Jiang H, and Rockman HA. Pathophysiology and pharmacology of G protein-coupled receptors in the heart. *Cardiovasc Res.* 2023;119(5):1117-29.
- Bhatt AS, DeVore AD, DeWald TA, Swedberg K, and Mentz RJ. Achieving a Maximally
   Tolerated beta-Blocker Dose in Heart Failure Patients: Is There Room for Improvement?
   JAm Coll Cardiol. 2017;69(20):2542-50.
- 708 6. Kim CW, Aronow WS, Dutta T, Frenkel D, and Frishman WH. Catecholaminergic Polymorphic Ventricular Tachycardia. *Cardiol Rev.* 2020;28(6):325-31.
- 710 7. Priori SG, Wilde AA, Horie M, Cho Y, Behr ER, Berul C, et al. HRS/EHRA/APHRS expert consensus statement on the diagnosis and management of patients with inherited primary arrhythmia syndromes: document endorsed by HRS, EHRA, and APHRS in May 2013 and by ACCF, AHA, PACES, and AEPC in June 2013. *Heart Rhythm*. 2013;10(12):1932-63.
- 715 8. Imberti JF, Underwood K, Mazzanti A, and Priori SG. Clinical Challenges in Catecholaminergic Polymorphic Ventricular Tachycardia. *Heart Lung Circ*. 2016;25(8):777-83.
- 718 9. Wootten D, Christopoulos A, and Sexton PM. Emerging paradigms in GPCR allostery: implications for drug discovery. *Nat Rev Drug Discov.* 2013;12(8):630-44.
- 720 10. Keov P, Sexton PM, and Christopoulos A. Allosteric modulation of G protein-coupled receptors: a pharmacological perspective. *Neuropharmacology*. 2011;60(1):24-35.
- 722 11. Christopoulos A. Allosteric binding sites on cell-surface receptors: novel targets for drug discovery. *Nat Rev Drug Discov.* 2002;1(3):198-210.
- 724 12. Whorton MR, Bokoch MP, Rasmussen SG, Huang B, Zare RN, Kobilka B, et al. A monomeric G protein-coupled receptor isolated in a high-density lipoprotein particle efficiently activates its G protein. *Proc Natl Acad Sci U S A*. 2007;104(18):7682-7.
- 727 13. Oakley RH, Laporte SA, Holt JA, Barak LS, and Caron MG. Molecular determinants underlying the formation of stable intracellular G protein-coupled receptor-beta-arrestin complexes after receptor endocytosis\*. *J Biol Chem.* 2001;276(22):19452-60.
- 730 14. Cahill TJ, 3rd, Thomsen AR, Tarrasch JT, Plouffe B, Nguyen AH, Yang F, et al. Distinct conformations of GPCR-beta-arrestin complexes mediate desensitization, signaling, and endocytosis. *Proc Natl Acad Sci U S A*. 2017;114(10):2562-7.
- 733 15. Shukla AK, Westfield GH, Xiao K, Reis RI, Huang LY, Tripathi-Shukla P, et al. Visualization of arrestin recruitment by a G-protein-coupled receptor. *Nature*. 2014;512(7513):218-22.
- 736 16. Rasmussen SG, DeVree BT, Zou Y, Kruse AC, Chung KY, Kobilka TS, et al. Crystal structure of the beta2 adrenergic receptor-Gs protein complex. *Nature*. 2011;477(7366):549-55.

- 739 17. Olsen RHJ, DiBerto JF, English JG, Glaudin AM, Krumm BE, Slocum ST, et al. TRUPATH, an open-source biosensor platform for interrogating the GPCR transducerome.

  741 *Nat Chem Biol.* 2020;16(8):841-9.
- 742 18. Namkung Y, Le Gouill C, Lukashova V, Kobayashi H, Hogue M, Khoury E, et al. 743 Monitoring G protein-coupled receptor and beta-arrestin trafficking in live cells using 744 enhanced bystander BRET. *Nat Commun.* 2016;7:12178.
- 745 19. Kim IM, Tilley DG, Chen J, Salazar NC, Whalen EJ, Violin JD, et al. Beta-blockers 746 alprenolol and carvedilol stimulate beta-arrestin-mediated EGFR transactivation. *Proc* 747 *Natl Acad Sci U S A*. 2008;105(38):14555-60.
- Wang J, Hanada K, Staus DP, Makara MA, Dahal GR, Chen Q, et al. Galpha(i) is required for carvedilol-induced beta(1) adrenergic receptor beta-arrestin biased signaling. *Nat Commun.* 2017;8(1):1706.
- Luttrell LM, Wang J, Plouffe B, Smith JS, Yamani L, Kaur S, et al. Manifold roles of beta arrestins in GPCR signaling elucidated with siRNA and CRISPR/Cas9. Sci Signal.
   2018;11(549).
- 754 22. Wang J, Pani B, Gokhan I, Xiong X, Kahsai AW, Jiang H, et al. beta-Arrestin-Biased Allosteric Modulator Potentiates Carvedilol-Stimulated beta Adrenergic Receptor Cardioprotection. *Mol Pharmacol.* 2021;100(6):568-79.
- 757 23. Kenakin T, and Strachan RT. PAM-Antagonists: A Better Way to Block Pathological Receptor Signaling? *Trends Pharmacol Sci.* 2018;39(8):748-65.
- Ahn S, Pani B, Kahsai AW, Olsen EK, Husemoen G, Vestergaard M, et al. Small-Molecule
   Positive Allosteric Modulators of the beta(2)-Adrenoceptor Isolated from DNA-Encoded
   Libraries. *Mol Pharmacol*. 2018;94(2):850-61.
- Pani B, Ahn S, Rambarat PK, Vege S, Kahsai AW, Liu A, et al. Unique Positive Cooperativity Between the beta-Arrestin-Biased beta-Blocker Carvedilol and a Small Molecule Positive Allosteric Modulator of the beta2-Adrenergic Receptor. *Mol Pharmacol*. 2021;100(5):513-25.
- Knollmann BC, Chopra N, Hlaing T, Akin B, Yang T, Ettensohn K, et al. Casq2 deletion causes sarcoplasmic reticulum volume increase, premature Ca2+ release, and catecholaminergic polymorphic ventricular tachycardia. *J Clin Invest.* 2006;116(9):2510-20.
- 770 27. Wleklinski MJ, Kannankeril PJ, and Knollmann BC. Molecular and tissue mechanisms of catecholaminergic polymorphic ventricular tachycardia. *J Physiol.* 2020;598(14):2817-34.
- Perez-Riera AR, Barbosa-Barros R, de Rezende Barbosa MPC, Daminello-Raimundo R,
   de Lucca AA, Jr., and de Abreu LC. Catecholaminergic polymorphic ventricular
   tachycardia, an update. *Ann Noninvasive Electrocardiol*. 2018;23(4):e12512.
- Peltenburg PJ, Kallas D, Bos JM, Lieve KVV, Franciosi S, Roston TM, et al. An International Multicenter Cohort Study on beta-Blockers for the Treatment of Symptomatic Children With Catecholaminergic Polymorphic Ventricular Tachycardia. *Circulation*. 2022;145(5):333-44.
- van der Werf C, Zwinderman AH, and Wilde AA. Therapeutic approach for patients with catecholaminergic polymorphic ventricular tachycardia: state of the art and future developments. *Europace*. 2012;14(2):175-83.
- 782 31. Wolfel A, Sattele M, Zechmeister C, Nikolaev VO, Lohse MJ, Boege F, et al. Unmasking 783 features of the auto-epitope essential for beta(1) -adrenoceptor activation by autoantibodies 784 in chronic heart failure. ESC Heart Fail. 2020;7(4):1830-41.

- 785 32. Bornholz B, Weidtkamp-Peters S, Schmitmeier S, Seidel CA, Herda LR, Felix SB, et al. Impact of human autoantibodies on beta1-adrenergic receptor conformation, activity, and internalization. *Cardiovasc Res.* 2013;97(3):472-80.
- 788 33. Freedman NJ, and Lefkowitz RJ. Anti-beta(1)-adrenergic receptor antibodies and heart failure: causation, not just correlation. *J Clin Invest.* 2004;113(10):1379-82.
- 790 34. Kew JN, Trube G, and Kemp JA. A novel mechanism of activity-dependent NMDA receptor antagonism describes the effect of ifenprodil in rat cultured cortical neurones. *J Physiol.* 1996;497 ( Pt 3)(Pt 3):761-72.
- Hudson BD, Christiansen E, Murdoch H, Jenkins L, Hansen AH, Madsen O, et al. Complex pharmacology of novel allosteric free fatty acid 3 receptor ligands. *Mol Pharmacol*.
   2014;86(2):200-10.
- 796 36. Price MR, Baillie GL, Thomas A, Stevenson LA, Easson M, Goodwin R, et al. Allosteric modulation of the cannabinoid CB1 receptor. *Mol Pharmacol*. 2005;68(5):1484-95.
- 798 37. Horswill JG, Bali U, Shaaban S, Keily JF, Jeevaratnam P, Babbs AJ, et al. PSNCBAM-1, 799 a novel allosteric antagonist at cannabinoid CB1 receptors with hypophagic effects in rats. 800 Br J Pharmacol. 2007;152(5):805-14.
- Fay JF, and Farrens DL. A key agonist-induced conformational change in the cannabinoid receptor CB1 is blocked by the allosteric ligand Org 27569. *J Biol Chem.* 2012;287(40):33873-82.
- 804 39. Krumm BE, DiBerto JF, Olsen RHJ, Kang HJ, Slocum ST, Zhang S, et al. Neurotensin Receptor Allosterism Revealed in Complex with a Biased Allosteric Modulator. *Biochemistry*. 2023;62(7):1233-48.
- 807 40. Sun D, Li X, Yuan Q, Wang Y, Shi P, Zhang H, et al. Molecular mechanism of the arrestin-808 biased agonism of neurotensin receptor 1 by an intracellular allosteric modulator. *Cell Res.* 809 2025;35(4):284-95.
- Strachan RT, Sun JP, Rominger DH, Violin JD, Ahn S, Rojas Bie Thomsen A, et al.
  Divergent transducer-specific molecular efficacies generate biased agonism at a G proteincoupled receptor (GPCR). *J Biol Chem.* 2014;289(20):14211-24.
- Shenoy SK, and Lefkowitz RJ. Receptor-specific ubiquitination of beta-arrestin directs assembly and targeting of seven-transmembrane receptor signalosomes. *J Biol Chem.* 2005;280(15):15315-24.
- Rockman HA, Choi DJ, Akhter SA, Jaber M, Giros B, Lefkowitz RJ, et al. Control of myocardial contractile function by the level of beta-adrenergic receptor kinase 1 in genetargeted mice. *J Biol Chem.* 1998;273(29):18180-4.
- Rohrer DK, Desai KH, Jasper JR, Stevens ME, Regula DP, Jr., Barsh GS, et al. Targeted disruption of the mouse beta1-adrenergic receptor gene: developmental and cardiovascular effects. *Proc Natl Acad Sci U S A*. 1996;93(14):7375-80.
- Yoo B, Lemaire A, Mangmool S, Wolf MJ, Curcio A, Mao L, et al. Beta1-adrenergic receptors stimulate cardiac contractility and CaMKII activation in vivo and enhance cardiac dysfunction following myocardial infarction. *Am J Physiol Heart Circ Physiol*. 2009;297(4):H1377-86.
- 46. Grogan A, Coleman A, Joca H, Granzier H, Russel MW, Ward CW, et al. Deletion of obscurin immunoglobulin domains Ig58/59 leads to age-dependent cardiac remodeling and arrhythmia. *Basic Res Cardiol*. 2020;115(6):60.

- 829 47. Rohrer DK, Chruscinski A, Schauble EH, Bernstein D, and Kobilka BK. Cardiovascular and metabolic alterations in mice lacking both beta1- and beta2-adrenergic receptors. *J Biol Chem.* 1999;274(24):16701-8.
- Curtis MJ, Hancox JC, Farkas A, Wainwright CL, Stables CL, Saint DA, et al. The Lambeth Conventions (II): guidelines for the study of animal and human ventricular and supraventricular arrhythmias. *Pharmacol Ther*. 2013;139(2):213-48.

# Acknowledgements

We thank Weili Zou for her invaluable technical assistance and Dr. Xinyu Xiong for his contributions to the generation of β<sub>1</sub>AR nanodiscs. We are also grateful to Dr. Sudar Rajagopal for the V<sub>2</sub>R-RLucII construct. Duke Cardiovascular Physiology Core provided expertise with implantation of telemetry monitors and real-time recording of ECG during the graded exercise experiments. We would like to thank Michael Chiaramonti, Research Assistant in the Rockman Lab, for his assistance with ECG analysis, and Dr. Darrion Rapoza, Senior Scientist at the Duke Cardiovascular Research Center, for his support with animal surgeries. We thank Dr. Ivan Spasojevic for directing experiments performed by the in vivo pharmacokinetics of C11 in the Duke Pharmacokinetics and Pharmacodynamics Shared Resource Core.

### **Funding**

This work is the result of NIH funding, in whole or in part, and is subject to the NIH Public Access Policy. Through acceptance of this federal funding, the NIH has been given a right to make the work publicly available in PubMed Central. This study was supported in part by the U.S. National Institutes of Health, National Heart, Lung, and Blood Institute grants (HL056687 to H.A.R.; HL16037 to R.J.L.), the Edna and Fred L. Mandel, Jr. Foundation (H.A.R), and the John Taylor Babbit Foundation and The Hartwell Foundation (A.P.L). The Duke Pharmacokinetics and Pharmacodynamics Shared Resource Core is supported by the National Cancer Institute Comprehensive Cancer Center Core Grant P30CA014236. R.J.L. is an investigator with the Howard Hughes Medical Institute (HHMI).

#### **Author contributions:**

- A.G., S.A., R.J.L., H.A.R., conceptualized the study. A.G., R.M.P., S.A., H.J., A.J., D.S., C.Y.,
- Q.C., J.L., J.W., A.W.K., developed the methodology. A.G., R.M.P., H.J., A.J., D.S., C.Y., J.W.,
- A.W.K., performed experiments. A.G., R.M.P., H.J., A.J., D.S., C.Y., Q.C., J.L., J.W., A.W.K.,
- analyzed data. J.S., R.J.L., H.A.R., provided resources and/or reagents. H.A.R acquired funding.
- 862 S.A., D.I.I., A.S., A.P.L., R.J.L., H.A.R., supervised the study. A.G. wrote the original draft of the
- manuscript. All authors reviewed, edited, and approved the manuscript for publication.

865

### **Competing interests:**

- A.G., R.M.P., S.A., H.J., A.J., J.W., A.W.K., A.P.L., R.J.L., and H.A.R. are co-inventors of patent
- application PCT/US24/39096 on Allosteric Modulators of the beta1-Adrenergic Receptor and
- methods of use, filed by Duke University. R.J.L. is a co-founder of Septerna, Inc., a company
- focused on the discovery and development of novel GPCR-targeted therapeutics and serves on the
- board of Lexicon Pharmaceuticals. H.A.R. and R.J.L. are co-founders of Trevena, Inc. S.A. and
- 871 R.J.L are shareholders of Septerna. The other authors declare no competing financial interests.

872

873

## **Supplementary Materials:**

- Materials and Methods
- 875 Supplementary Figures 1-9
- 876 Supplementary Tables 1-4
- 877 References
- 878 Supporting Data Values

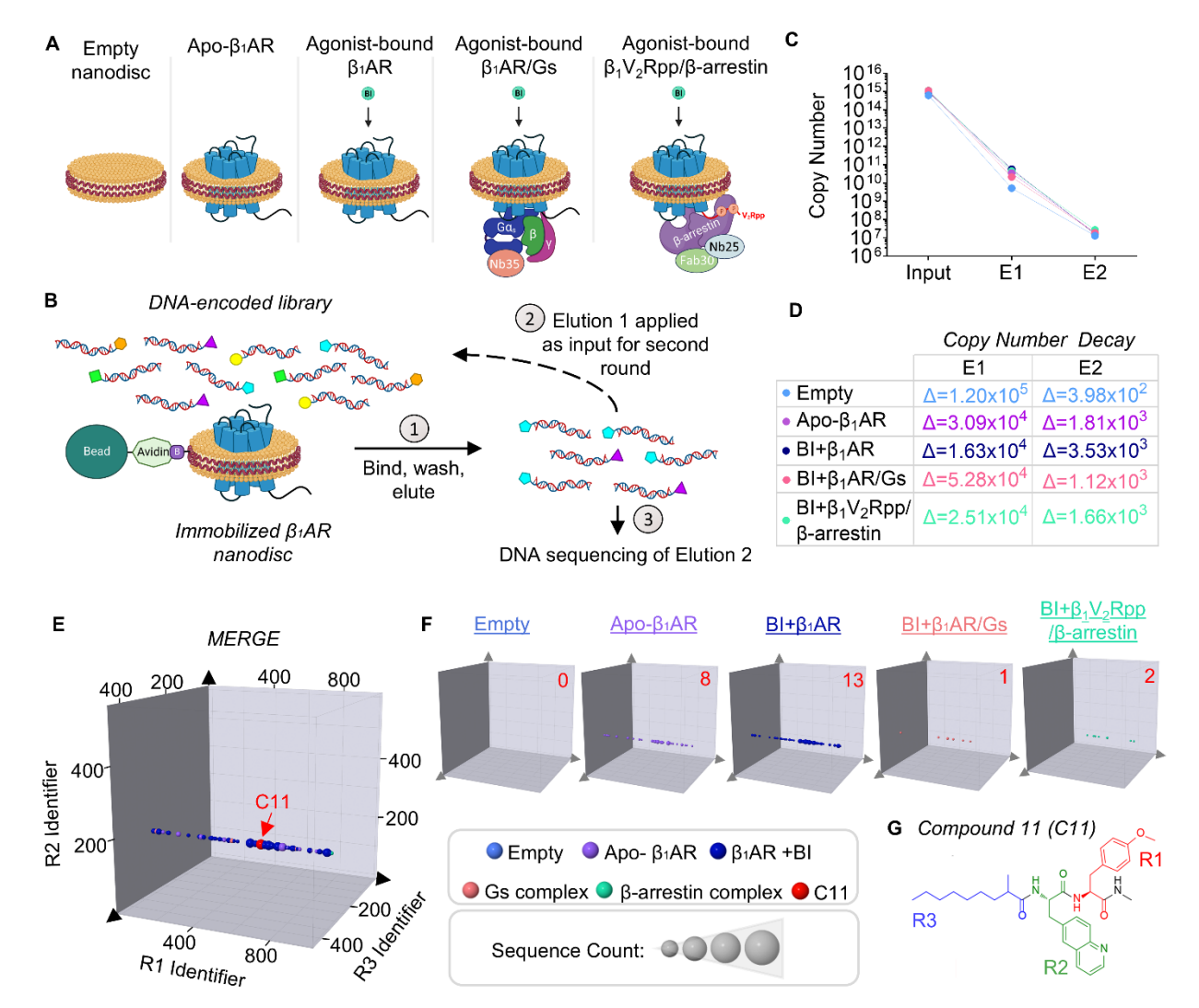


Fig. 1. Discovery of C11 through DNA-encoded small molecule library (DEL) screening. (A) Schematic of screening conditions including the empty nanodisc and un-liganded (apo)-β1AR nanodisc controls, β<sub>1</sub>AR nanodiscs bound to the high-affinity orthosteric agonist, BI-167107 (BI), and BI-bound  $\beta_1AR$  or  $\beta_1V_2Rpp$  in complex with transducers (heterotrimeric  $G_s$  or  $\beta$ -arrestin 1, respectively). Transducer complexes were further reinforced using conformation-stabilizing nanobodies Nb35 (included in β<sub>1</sub>AR/G protein complex), Nb25, and Fab30 (included in β<sub>1</sub>V<sub>2</sub>Rpp/β-arrestin complex). (B) Purified β<sub>1</sub>ARs reconstituted in biotinylated lipid nanodiscs were immobilized using neutravidin beads and incubated with HitGen's OpenDEL<sup>TM</sup> small molecule library. Following washing, bound compounds were eluted (Elution 1) and applied as input for a second round of affinity selection with fresh  $\beta_1AR$  nanodiscs. Molecules from the final elution (Elution 2) were identified by high-throughput DNA sequencing. (C-D) DNA copy number in eluted samples (E1-2) was determined by qPCR following each round of affinity selection. Compared to library input ( $\sim 10^{15}$  molecules), copy number was reduced to  $\sim 10^7$  following two rounds of screening in each condition (C). Approximately 10<sup>4-5</sup> molecules were lost in round 1 and  $\sim 10^{2-3}$  were lost in round 2 (D). (E-F) 3-dimensional plots of each screening condition (F) and all five conditions merged (E) depict an enriched chemical line feature where C11 was identified. This line feature was enriched in Apo-β<sub>1</sub>AR and BI-β<sub>1</sub>AR samples, minimally present in transducer

882

883

884

885

886

887

888 889

890

891

892

893

894 895

896

complex samples and completely absent in the empty nanodisc condition. Axes enumerate the chemical building blocks utilized in each round of chemical synthesis (R1-R3). Data point size corresponds to the sequence count for a particular compound, and the copy number of C11 in each condition is indicated in red text. Compounds outside of the feature that contains C11 were filtered out to facilitate visualization of the enriched chemotype. (G) Schematic of the chemical structure of C11 generated through three rounds of chemical synthesis: R1, red; R2, green; R3, blue.

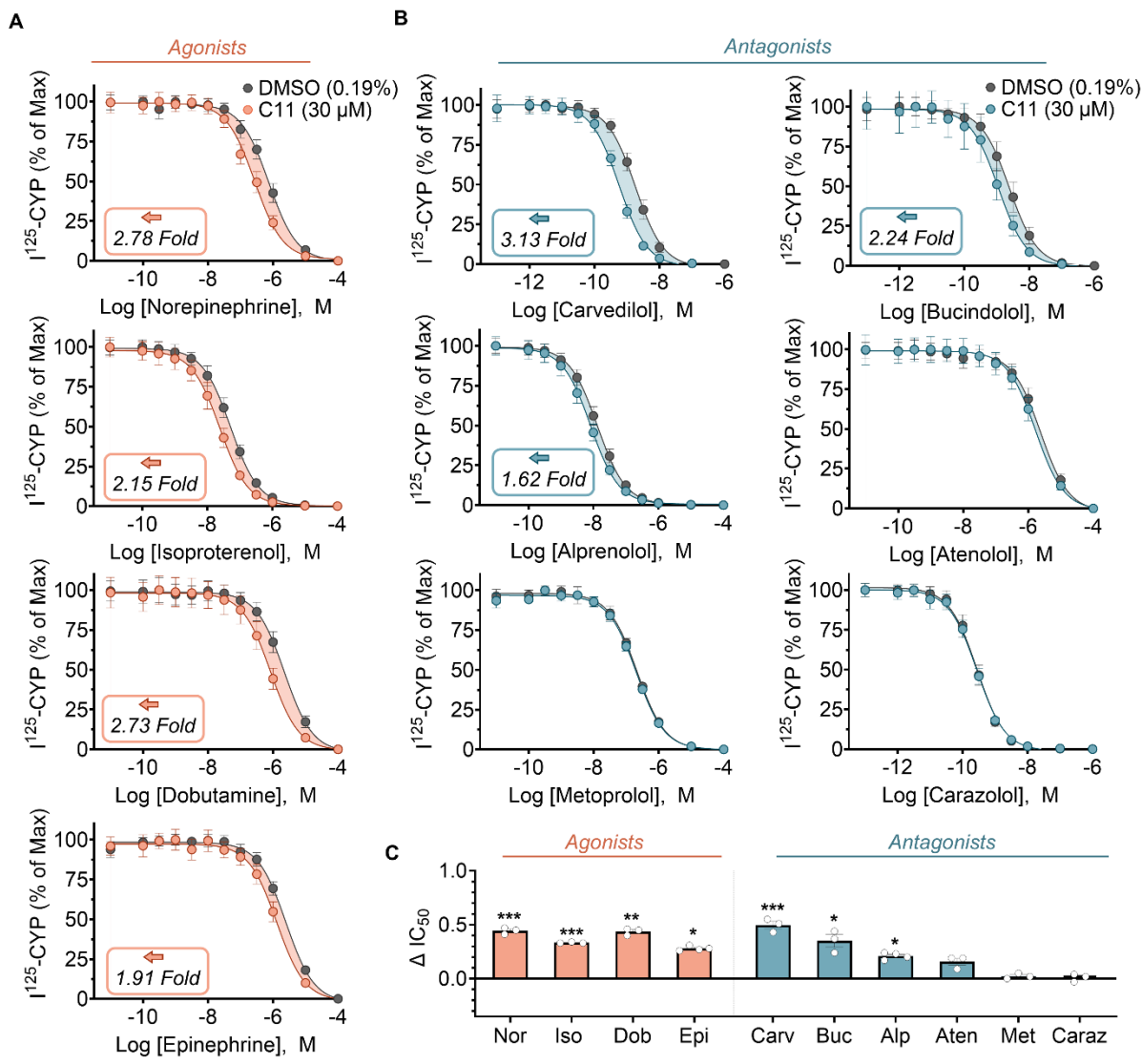


**Fig. 2.** C11 potentiates the binding affinity of agonists and a subset of antagonists to the  $β_1AR$ . (A-C)  $β_1AR$  nanodiscs were incubated with a fixed amount of radiolabeled orthosteric antagonist,  $I^{125}$ -CYP, serial doses of unlabeled orthosteric ligand, and either DMSO (0.19%) or 30 μM C11. The resulting competition binding curves (A-B) and corresponding  $IC_{50}$  shift quantifications (C) revealed that C11 enhanced the binding affinity of agonists (norepinephrine, Nor; isoproterenol, Iso; dobutamine, Dob; and epinephrine, Epi) and a subset of antagonists (carvedilol, Carv; bucindolol, Buc; alprenolol, Alp) to the  $β_1AR$  with no effect on the binding affinity of the antagonists atenolol (Aten), metoprolol (Met) or carazolol (Caraz). Dose-response curves are presented as percent of maximum  $I^{125}$ -CYP binding.  $IC_{50}$  values were calculated from the nonlinear fit (one-site binding; GraphPad prism) and plotted as the difference between  $IC_{50}$  (DMSO) and  $IC_{50}$  (C11). Raw  $IC_{50}$  values are presented in Supplemental Table 1. F-tests were performed on the non-linear fit; \*p<0.05, \*\*p<0.01, \*\*\*p<0.001; data points represent mean ± SEM of at least 3 independent experiments performed in duplicate.

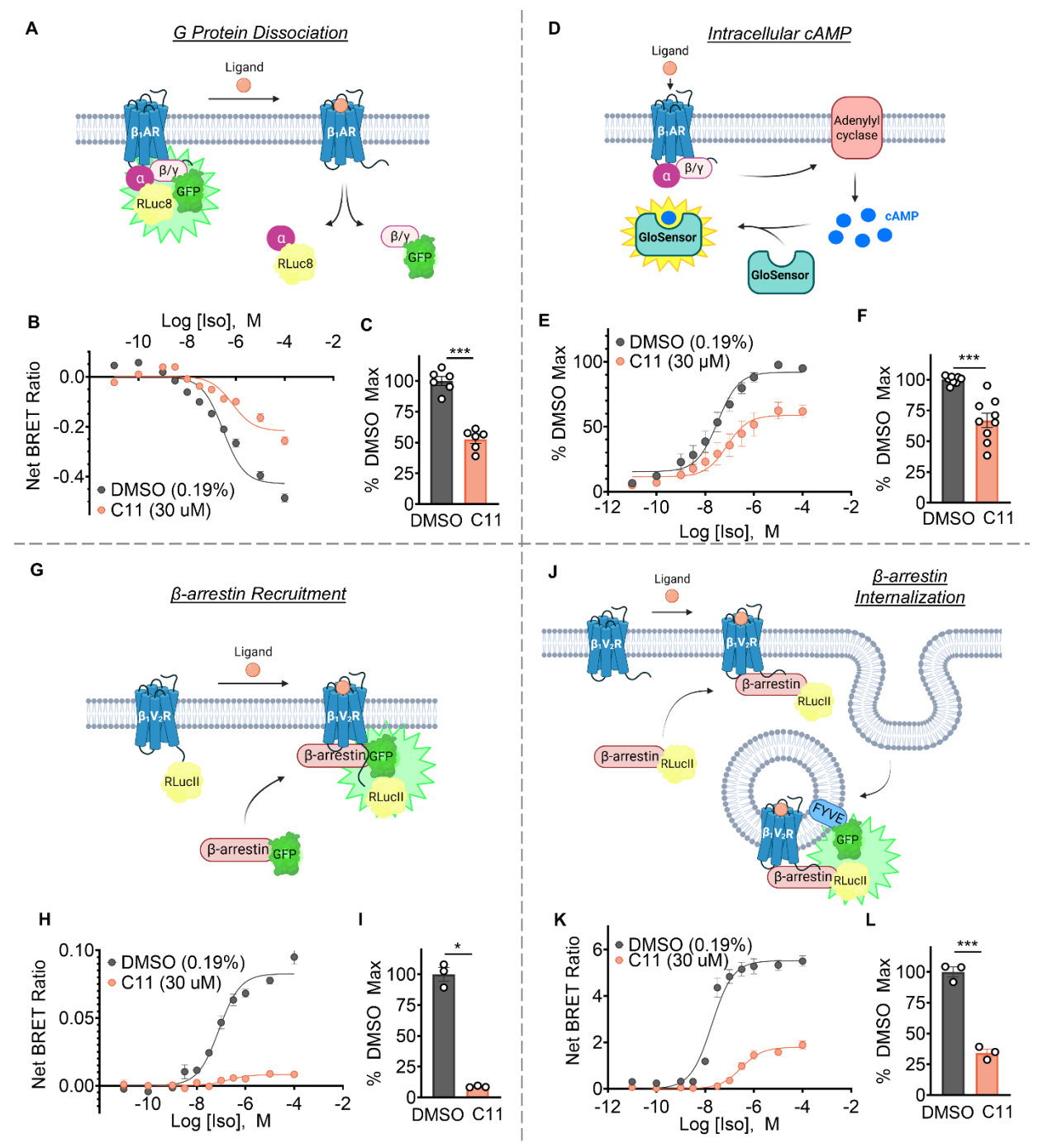


Fig. 3. C11 suppresses G protein signaling and  $\beta$ -arrestin function downstream of agonist-activated  $\beta_1AR$  in HEK293T cells. (A-L) HEK293T cells transiently transfected with  $\beta_1AR$  (or  $\beta_1V_2R$ ) and BRET or luciferase biosensor plasmids were pre-treated with DMSO (0.19%) or 30  $\mu$ M C11 and then stimulated with serial doses of the agonist isoproterenol (Iso). Schematic representation of the BRET-based Trupath G protein dissociation assay where  $G\alpha_s$ -RLuc8 dissociates from  $G\beta/G\gamma$ -GFP upon  $\beta_1AR$  activation, resulting in BRET signal decay (A). C11 treatment significantly reduced maximal G protein dissociation compared to vehicle (B-C). Schematic representation of the GloSensor luciferase-based biosensor that emits light in response to binding intracellular cAMP (D). C11 treatment significantly reduced maximal cAMP

accumulation compared to vehicle (E-F). Schematic representation of the BRET-based  $\beta$ -arrestin recruitment assay wherein  $\beta$ -arrestin-GFP is recruited to  $\beta_1 V_2 R$ -RLucII upon receptor activation and generates a BRET signal (G). C11 treatment significantly reduced maximal  $\beta$ -arrestin recruitment to  $\beta_1 V_2 R$ -RLucII compared to vehicle (H-I). Schematic representation of BRET-based  $\beta$ -arrestin-mediated receptor internalization assay (J). Upon  $\beta_1 V_2 R$  activation, the receptor/ $\beta$ -arrestin-RLucII complex is internalized into endosomes and a BRET signal is generated when internalized  $\beta$ -arrestin-RLucII and endosomal marker FYVE-GFP are in proximity. C11 treatment significantly reduced maximal  $\beta$ -arrestin internalization compared to vehicle (K-L); F-test, \*p<0.05, \*\*\*p<0.001; data points represent mean  $\pm$  SEM of at least 3 independent experiments performed in duplicate or quadruplicate; curve fits were plotted using a log(agonist) three-parameter model in GraphPad Prism; net BRET ratios (emission of RLuc8/GFP) are baseline-subtracted according to the non-linear fit of each treatment condition; luminescence values and Emax quantifications (derived from the non-linear fit) are presented as the percent of maximal signal in the vehicle condition.

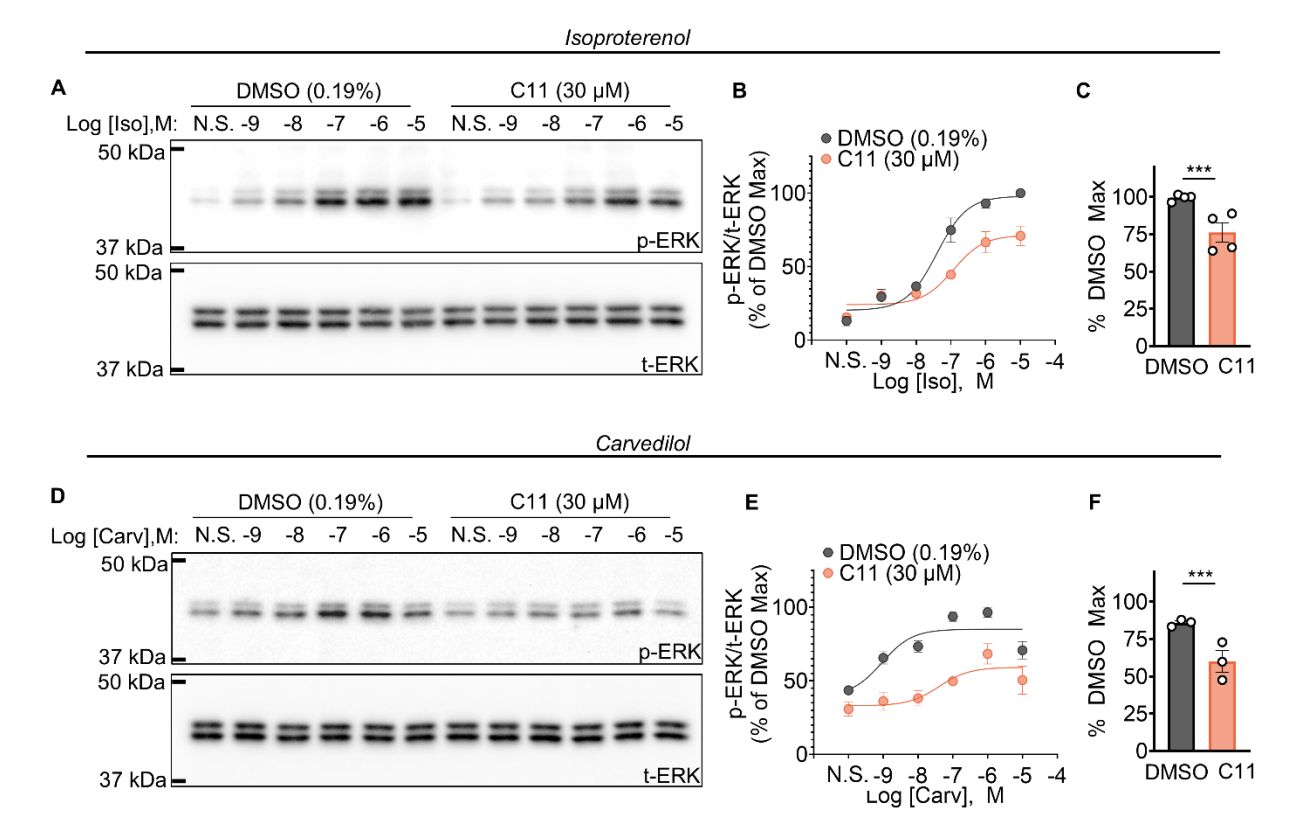


Fig. 4. C11 suppresses phosphorylation of ERK mediated by isoproterenol or carvedilol downstream of agonist-activated  $\beta_1AR$  in HEK293T cells. (A-C) Representative immunoblots (A), relative densitometry quantifications (B) and Emax values of the nonlinear curve fit (C) demonstrated that C11 significantly reduced maximal ERK phosphorylation (pERK) in response to isoproterenol (Iso) compared to vehicle control in HEK293T cells transiently expressing the  $\beta_1AR$ . (D-F) Representative immunoblots (D), relative densitometry quantifications (E) and Emax values of the nonlinear curve fit (F) demonstrated that C11 significantly reduced maximal pERK in response to carvedilol (Carv) compared to vehicle control in HEK293T cells transiently expressing  $\beta_1AR$ ; densitometric values of pERK were normalized to total ERK (tERK) and presented as percent of the maximal value in vehicle-treated cells; F-test, \*\*\*p<0.001; data points represent mean  $\pm$  SEM of at least 3 independent experiments; nonlinear curve fits and Emax values were calculated from a log(agonist) three-parameter model in GraphPad Prism.

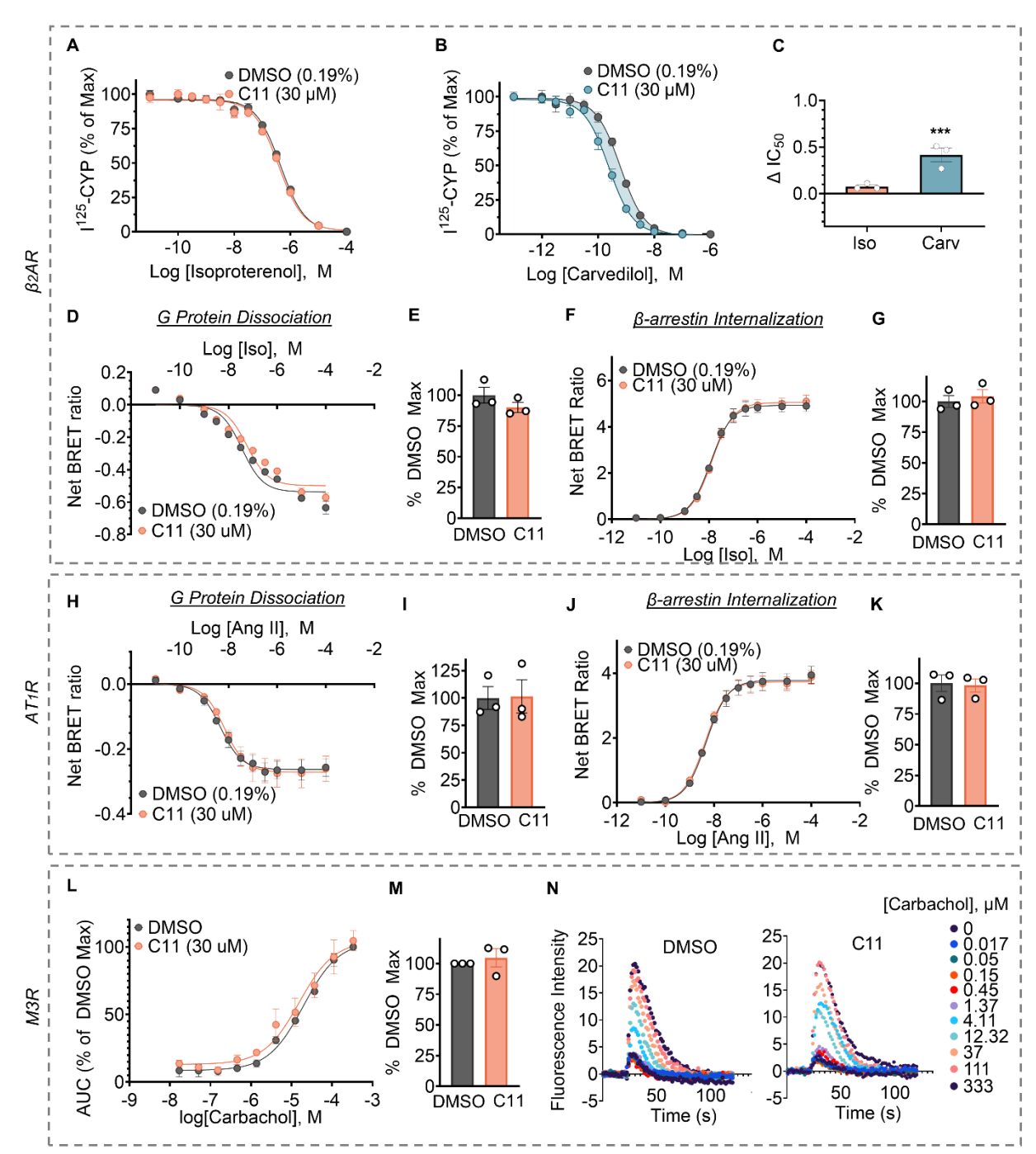


Fig. 5. C11 does not suppress cellular signaling mediated by alternative receptors  $\beta_2AR$ , AT1R, or M3R. (A-C)  $\beta_2AR$  nanodiscs were incubated with a fixed amount of radiolabeled orthosteric antagonist, I<sup>125</sup>-CYP, serial doses of unlabeled orthosteric ligand, and either vehicle or 30  $\mu$ M C11. Competition binding curves (A-B) and corresponding IC<sub>50</sub> shifts (C) revealed that C11 enhanced the binding affinity of carvedilol (Carv) to the  $\beta_2AR$ , but not isoproterenol (Iso). Dose response curves are presented as percent of maximum I<sup>125</sup>-CYP binding. IC<sub>50</sub> values were calculated from the nonlinear fit (one-site binding; GraphPad Prism) and plotted as the difference between IC<sub>50</sub> (DMSO) and IC<sub>50</sub> (C11). F-tests were performed on the non-linear fit; \*\*\*p<0.001. Data points represent mean  $\pm$  SEM of at least 3 independent experiments performed in duplicate.

(D-K) HEK293T cells transiently overexpressing receptor ( $\beta_2AR$ ,  $\beta_2V_2R$ , or AT1R) and BRET fusion proteins (Fig. 3A; Fig. 3J) were pre-treated with vehicle or 30  $\mu$ M C11 and stimulated with either isoproterenol (for  $\beta_2AR$  or  $\beta_2V_2R$ ) or angiotensin II (Ang II, for AT1R). C11 treatment had no significant effect on G-protein dissociation or  $\beta$ -arrestin internalization downstream of agonist-activated  $\beta_2AR/\beta_2V_2R$  (D-G), or AT1R (H-K). (L-N) HEK293T cells pre-treated with vehicle or 30  $\mu$ M C11 were stimulated with carbachol to activate the endogenous  $G_q$ -coupled muscarinic M3 receptor (M3R). C11 treatment had no significant effect on the resulting Ca<sup>2+</sup> response (L-M). Representative time-course plots of the baseline-subtracted raw fluorescence at each carbachol dose depicted comparable Ca<sup>2+</sup> responses between vehicle- and C11- treated cells (N); data points represent mean  $\pm$  SEM of at least 3 independent experiments performed in duplicate or triplicate; curve fits were plotted using a log(agonist) three-parameter model in GraphPad Prism; net BRET ratios (emission of RLuc8/GFP) are baseline-subtracted according to the non-linear fit of each treatment condition. Ca<sup>2+</sup> responses are presented as the baseline-subtracted area under the curve (AUC) and normalized to the percent of DMSO maximum.

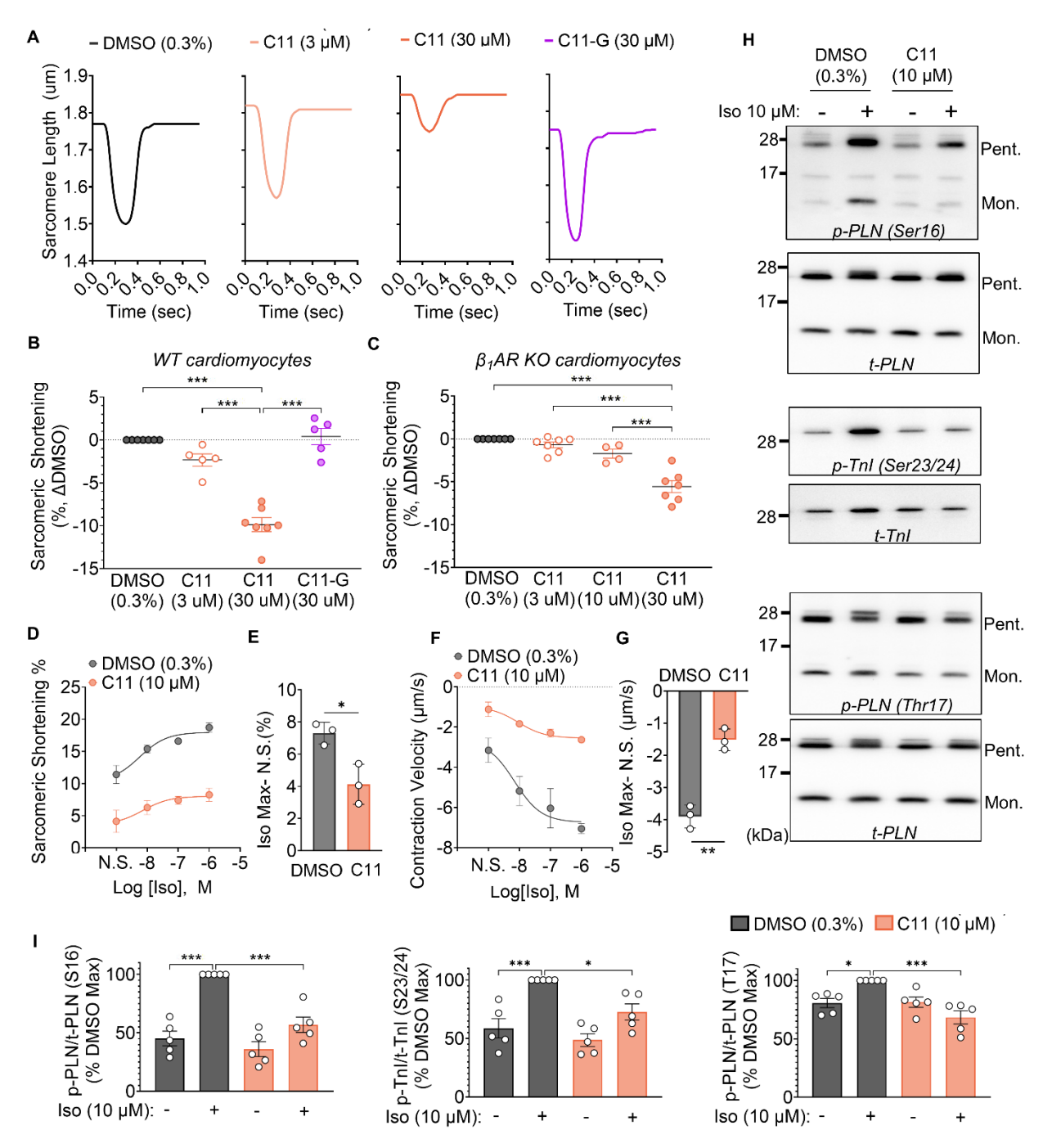


Fig 6. C11 reduces basal contractility and suppresses the isoproterenol response in isolated wild-type cardiomyocytes. (A-B) Representative unloaded shortening contractions (A) from isolated wild-type cardiomyocytes treated with increasing doses of C11 displayed a significant decrease in basal sarcomeric shortening in cardiomyocytes treated with 30  $\mu$ M C11 compared to vehicle, whereas treatment with 'loss of function' C11 analog, C11-G, had no effect (B). (C) High doses of C11 (30  $\mu$ M) also elicited a significant reduction in basal sarcomeric shortening in  $\beta_1 AR^{-1}$  cardiomyocytes, indicating that the C11-mediated reduction in contractility is partially non-selective. An intermediate dose of 10  $\mu$ M was therefore selected for functional cardiomyocyte assays; one-way ANOVA, \*\*\*p<0.0002; data points represent biological replicates (n = 4-7 hearts,

7-10 cells per treatment per heart); absolute measurements of all contractility parameters are included in Supplemental Table 3 (D-G) The dose-dependent enhancement of sarcomeric shortening (D) and contraction velocity (F) stimulated by serial doses of isoproterenol (Iso) was significantly blunted (E, G) in isolated wild-type cardiomyocytes treated with 10 µM C11 compared to vehicle-treated cells. The magnitude of the isoproterenol-mediated increase is plotted as the difference between maximal isoproterenol dose (Log[Iso] = -6 M) and the non-stimulated (N.S.) condition (E, G); t-test, \*p<0.05, \*\*p<0.01; data points represent the mean  $\pm$  SEM of n = 3 biological replicates (7-10 cells per treatment per heart). (H-I) Representative immunoblots (H) and corresponding densitometric quantifications (I) revealed significantly decreased levels of phosphorylated PLN (Ser16), TnI (Ser23/24), and PLN (Thr17) in C11-treated cardiomyocytes (10 µM) compared to vehicle control following isoproterenol stimulation. Phosphorylated proteins (pPLN and pTnI) are normalized to total levels (tPLN and tTnI). Statistical comparisons (one-way ANOVA) are shown between DMSO(vehicle) and DMSO(iso), C11(vehicle) and C11(iso), and between DMSO(iso) and C11(iso) groups only; \*p<0.03, \*\*p<0.002, \*\*\*p<0.0002; data points represent biological replicates (n = 5 hearts, each performed in duplicate); WT, wild-type; Pent, pentamer; Mon, monomer.

993

994

995

996

997

998

999 1000

1001

1002

1003

1004

1005

1006

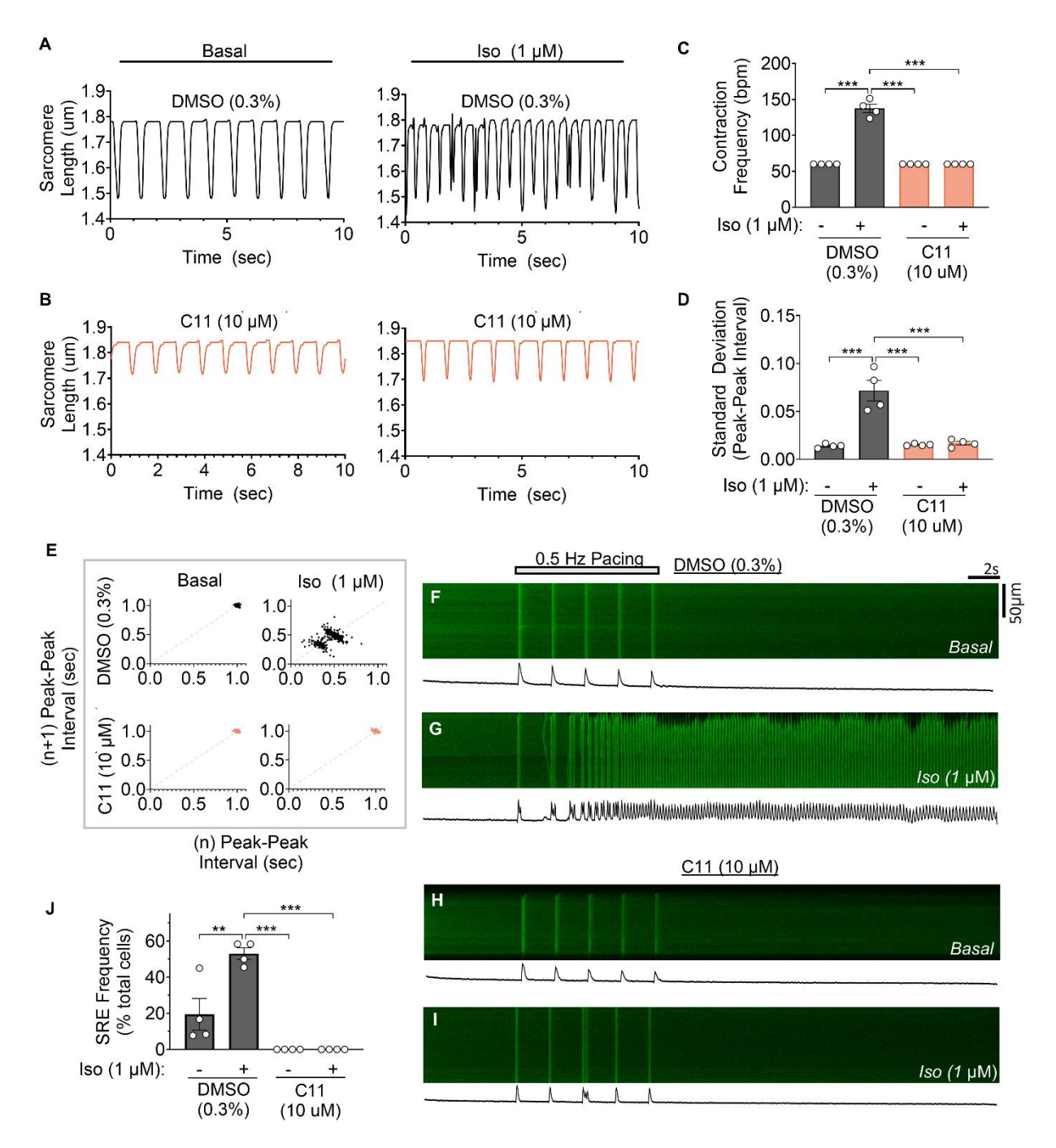


**Fig 7. C11 restores regular contractile rhythm and suppresses spontaneous Ca<sup>2+</sup> release events in cardiomyocytes isolated from CSQ2<sup>-/-</sup> mice. (A-D) Representative unloaded shortening contractions (A-B) and corresponding quantifications (C-D) revealed frequent and irregular beats in vehicle-treated CSQ2<sup>-/-</sup> cardiomyocytes stimulated with isoproterenol (Iso) during 1Hz pacing (i.e. 1 sec interval), reminiscent of ventricular tachycardia. Remarkably, isoproterenol-mediated spontaneous beating is completely attenuated in cells pre-treated with 10 μM C11; data points represent biological replicates (n = 4 hearts, 7-10 cells per treatment per heart); one-way ANOVA, \*\*\*\*p<0.0002. (<b>E**) Poincaré plots depict increased variability in the interval between consecutive cellular contractions in vehicle-treated CSQ2<sup>-/-</sup> cardiomyocytes

stimulated with isoproterenol but not in cells pre-treated with 10  $\mu$ M C11; data points represent peak-peak intervals of all biological replicates combined. (F-J) Spontaneous Ca<sup>2+</sup> release events (SREs) were measured in quiescent ventricular cardiomyocytes following pacing at 0.5Hz. Representative confocal line scans with associated fluorescent intensity profiles (F-I) and corresponding quantifications (J) revealed a robust increase in spontaneous Ca<sup>2+</sup> release event frequency in vehicle-treated CSQ2<sup>-/-</sup> cardiomyocytes after stimulation with isoproterenol (Iso, G) that was significantly attenuated in cells pre-treated with 10  $\mu$ M C11 (I); data points represent biological replicates (n = 4 hearts, 11-13 cells per treatment per heart); one-way ANOVA, \*\*p<0.0013, \*\*\*p<0.0002.

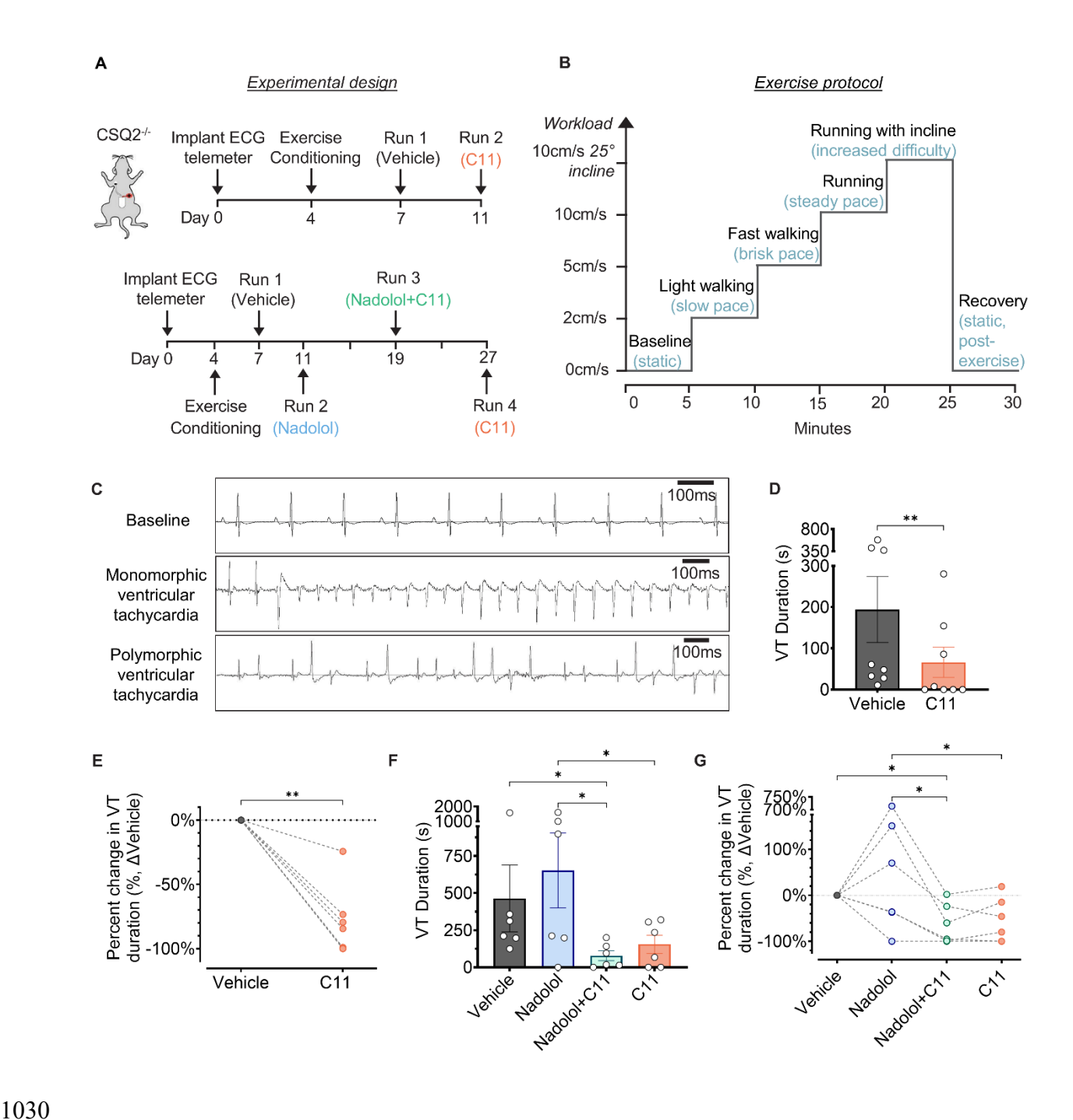


**Fig 8. C11 suppresses the duration of exercise-induced ventricular tachycardia** *in vivo*. **(A)** CSQ2<sup>-/-</sup> mice were implanted with telemetry devices (day 0) and allowed to recover for 3 days prior to acclimation (days 4-6). Mice were pre-treated with vehicle (day 7) or 10 mg/kg C11 (day 11) and subjected to a strenuous treadmill exercise protocol (upper panel). For combination experiments with nadolol (lower panel), mice were allowed a 7-day washout between drug treatments. **(B)** Illustrative graph of the 30-minute graded exercise protocol where workload (i.e. speed and incline) was incrementally increased every 5 minutes. Mice were placed on a single-lane treadmill with an adjustable incline (maximum 25°). Vehicle or drug solutions were administered intraperitoneally 45 minutes before exercise began. **(C)** Representative

electrocardiograms obtained via continuous telemetric recording depict normal sinus rhythm at rest (baseline) and episodes of monomorphic and/or polymorphic ventricular tachycardia (VT) in CSQ2<sup>-/-</sup> mice during physical exertion. **(D)** The total duration of VT was significantly reduced in CSQ2<sup>-/-</sup> mice pre-treated with C11 compared to when these same mice were pre-treated with vehicle during exercise; data points represent biological replicates (n = 8 mice); Wilcoxon matched pairs signed rank test, \*\*p<0.01. **(E)** The percent change in total VT duration after C11 treatment compared to vehicle was plotted for individual mice. **(F)** VT duration was measured in a separate cohort of CSQ2<sup>-/-</sup> mice treated sequentially with vehicle solution (Day 7), low-dose nadolol (0.01 mg/kg; Day 11), combination of low-dose nadolol (0.01 mg/kg) and C11 (10 mg/kg; Day 19), and C11 alone (10 mg/kg; Day 27). The average VT duration was significantly lower when treated with C11 alone or in combination with low-dose nadolol compared to nadolol alone. **(H)** The percent change in total VT duration after each treatment was plotted for individual mice; data points represent biological replicates (n = 6 mice); non-parametric repeated measures one-way ANOVA (Friedman's test), \*p<0.05.